Microchim Acta (2012) 177:245–270
DOI 10.1007/s00604-011-0758-1

REVIEW ARTICLE

Electrochemical biosensing based on noble metal nanoparticles

Jing Wang

Received: 13 October 2011 / Accepted: 27 December 2011 / Published online: 13 January 2012

Abstract The interest in the fabrication of electrochemical biosensors with high sensitivity, selectivity and efficiency is rapidly growing. In recent years, noble metal nanoparticles (NMNPs), with extraordinary conductivity, large surface-to-volume ratio and biocompatibility, have been extensively employed for developing novel electrochemical sensing platforms and improving their performances. Through distinct surface modification strategies (e.g. self-assembly, layer-by-layer, hybridization and sol-gel technology), NMNPs provide well control over the microenvironment of biological molecules retaining their activity, and facilitate the electron transfer between the redox center of biomolecules and electrode surface. Moreover, NMNPs have been involved into biorecognition events (e.g. immunoreactions, DNA hybridization and ligand-receptor interactions) by conjugating with various biomolecules, chemical labels and other nanomaterials, achieving the signal transduction and amplification. The aim of this review is to summarize different strategies for NMNP-based signal amplification, as well as to provide a snapshot of recent advances in the design of electrochemical biosensing platforms, including enzyme/protein sensors focused on their direct electrochemistry on NMNP-modified electrode surface; immunosensors and gene sensors in which NMNPs not only participate into biorecognition, but also act as electroactive tags to enhance the signal output. In addition, NMNP alloy-based multifunctional electrochemical biosensors are briefly introduced in terms of their unique heterostructures and properties.

J. Wang (✉)
Department of Chemistry and Photonics Center,
Boston University,
Boston, MA 02215, USA
e-mail: jennyw@bu.edu

Keywords Biosensors · Direct electron transfer · Electrode modification · Genesensors · Immunosensors · Noble metal nanoparticles · Protein immobilization · Signal amplification

Introduction

Biosensors, with their practical advantages of high selectivity, sensitivity and simple manipulation, have attracted broad research interest and undergone rapid development. In recent years, it has become one of the most important research areas ranging from medical analysis, environmental monitoring, to battlefield detection of warfare agents. A biosensor typically contains three components: the biological element recognizing analyte in the sample; the transducer/detector element transforming the signal generated from the biological interaction into another signal which can be more easily measured and quantified; the associated signal processors primarily responsible for the display of the results in a user-friendly way. Among various species of biosensors (optical, thermal, acoustic etc.), electrochemical biosensors are of special interest due to their analytical characteristics including operational simplicity, extraordinary sensitivity, low cost and rapid, real-time detection. In recent years, intensive research effort has been put into the design of novel electrochemical biosensors as well as the improvement of their performances.

Nanomaterials such as noble metal nanoparticles (NMNPs), inorganic nanotubes/nanowires, and semiconductor quantum dots exhibit unique electronic, optical, thermal and catalytic properties [1]. Especially NMNPs (mainly gold (AuNPs), silver (AgNPs), platinum (PtNPs), palladium (PdNPs), ruthenium (RuNPs) and their alloy Au-Ag, Au-Pt, Ag-Pt, Pt-Pd, etc.) possess exceeding advantages over other nanomaterials including stability, conductivity, biocompatibility, low

cytotoxicity and size-related electronic, magnetic and optical properties [2–6]. For the fabrication of electrochemical biosensors, the dimensional similarities of NMNPs with biological molecules and large surface areas provide opportunities for the stable immobilization of biomolecules with their bioactivity maintained; and their conductivity facilitates the electron transfer between biological elements and electrode surface. Additionally, the stability and biocompatibility of NMNPs make them easy to conjugate multiple species of biomolecules, chemical groups and polymer materials. Besides, the unique electrocatalytic activity of some NMNPs (e.g. PtNPs) could be employed to design label-free electrochemical sensors.

Due to the significant role of NMNPs in the biosensor fabrication, how to prepare NMNPs with appropriate size, shape, assembly and surface modification becomes primary element which determines the performance of a biosensor. In general, the synthesis of NMNPs involves the chemical reduction of noble metal salt in aqueous or organic phase. However, the high surface energy of NMNPs makes them extremely unstable and easy to undergo aggregation without protection or passivation of their surfaces. As a result, NMNPs are typically synthesized in the presence of a stabilizer/surface protector which binds onto particle surface to improve their stability and solubility, as well as provide charge and chemical groups. The preparation of colloidal AuNPs through the reduction of chloroauric acid ($HAuCl_4$) by sodium citrate in aqueous media is the most commonly used method, and the stabilizer ranges from ions, small molecules, polymers to multiple kinds of biological molecules. Some nicely written reviews are available introducing variable methods of AuNP synthesis and surface modification [7]. Compared with AuNPs, AgNPs possess larger scattering cross section and unique capabilities to amplify certain behaviors such as Raman scattering [8, 9] and fluorescence [10, 11]. However, the preparation of monodisperse AgNPs is more challenging due to its propensity of corrosion and aggregation in electrolytic solution [12]. In 1997, Taleb et al. synthesized highly monodisperse AgNPs in the liquid phase for the first time [13], starting from an initial synthesis in a surfactant system consisted of functionalized dioctyl sodium sulfosuccinate reverse micelles. To narrow the particle size distribution, the particles were extracted from the micellar solution. More frequently used water-soluble AgNPs are prepared through the reduction of silver nitrate ($AgNO_3$) by sodium borohydride ($NaBH_4$) and stabilized by citrate [14, 15], polymer (e.g. polyethylene glycol) [16] and biological molecules (e.g. peptide and DNA) [17, 18]. These proper protective layers are able to maintain the stability of AgNPs at high salt concentrations over a wide range of pH. PtNPs with different sizes, shapes and structures exhibit distinctive capability in catalyzing oxidation, hydrogenation and dehydrogenation of a variety of molecules. The commonly used precursors for synthesizing PtNPs can be chosen from hexachloroplatinic acid (H_2PtCl_6), potassium hexachloroplatinate (K_2PtCl_6), potassium tetrachloroplatinate (K_2PtCl_4), to platinum acetylacetonate ($Pt(acac)_2$), depending on the choice of solvents (either water or organic liquids), reductants (e.g. borohydride, hydrazine, hydrogen, citrate, and ascorbic acid), surfactants (e.g. poly (N-vinyl-2-pyrrolidone) and hexadecyltrimethylammonium bromide), and other additives [19]. The easiest water-phased synthesis of PtNPs is similar to AuNPs, using the reduction of H_2PtCl_6 by sodium citrate [20]. And the modification of biological molecules through Pt-thiol bond is becoming an effective alternative to enhance the stability of PtNPs [21]. It has to be mentioned that although the synthesis of NMNPs makes great progress, it is still a challenge to precisely control their monodisperse properties, morphology, and surface chemistry.

The aim of this review is to summarize frequently-used methods for surface modification on substrate electrodes using NMNPs (mainly AuNPs, AgNPs, PtNPs and their alloy), which increase the immobilization efficiency of biological molecules and accelerate the electron transfer rate on electrode surface. Furthermore, some of NMNP-based signal amplification strategies are illustrated, it which NMNPs provide elegant ways for the biomolecular recognition with electrochemical signal transduction and enhancement. After that the recent advances in the fabrication of NMNP-based electrochemical biosensors are listed, including 1) direct electron transfer (DET) of redox proteins/enzymes on NMNP-modified electrode surface; 2) NMNP-based single/multi-analyte immunosensors for the detection of tumor markers, bacteria/virus and living cells; 3) genesensors, which are divided into label-free sensors *via* direct oxidation of DNA bases on NMNP-modified electrode surface, and indirect sensors utilizing NMNPs for signal amplification. Since there are some nice review articles in the recent years introducing the development of metal and semi-conductor nanomaterial-based biosensors [22–25], this review mainly focuses on the original research articles from 2009 to 2011. Some articles detailing important advances in this field might be left out, and the author apologizes for these inevitable oversights.

NMNP-based surface modification methods

The modification of electrode surface with sophisticated molecular assembly is one of the foundations for the fabrication of an electrochemical biosensor. There has been intense interest in developing novel molecular architecture based on nanomaterial constructs, biomolecules and numbers of organic/inorganic materials. They are utilized to facilitate electron transfer, control reactions on the electrode surface, tailor surface properties and provide additional functionalities. Here we will introduce four typical surface modification methods with the involvement of NMNPs,

which are either directly assembled onto electrode surface, or integrated with other materials to form complicated structures.

Self-assembly monolayer

Self-assembled monolayer (SAM) provides an organized layer of amphiphilic molecules (containing a functional group on one end and a head group on the other) due to the specific and strong chemisorption of head groups onto the electrode surface [26]. The performances of SAM-modified electrodes are variable based on the characteristics of functional groups [27]. The frequently used SAMs for electrochemistry are based on the affinity between thiols/amines and noble metal surfaces. As a consequence, the well-ordered NMNP monolayers formed by S-/NH-noble metal bonds can be used to immobilize biological molecules with a high degree of control over the molecular architecture of the recognition interface. Recent works have demonstrated that the immobilization of NMNPs on bulk electrode by SAM strategies provides a simple, fast and versatile approach for preparing biocompatible electrode surfaces with strong electron transfer capacity and low background signal [28]. The possibility of altering particle size and density by controlling particle synthesis condition further enhances the attractiveness of NMNP-modified interfaces for sensing applications [29]. For instance, a cysteamine SAM could be formed on gold electrode surface through thiol-gold bond, and then covered by an AuNP seed (diameter 3.5 nm) monolayer through the electrostatic interaction between positively-charged amino groups of cysteamine and citrate-protective AuNPs [30]. After that, cholesterol oxidase could be immobilized through self-adsorption *via* coordinate-covalent bond between amino groups of protein and AuNP surface. The SAM of AuNP seeds had two distinct functions: when the size was small, their excellent conductivity and biological compatibility made the cholesterol oxidase keep bioactivity. In the presence of $HAuCl_4$ and cholesterol, the byproduct H_2O_2 generated by enzyme catalysis resulted in the reduction of Au^{3+} ion to Au atom, subsequently the enlargement of AuNPs with up to 50 nm diameter. These larger-sized AuNPs covered on the electrode surface densely and blocked the electronic communication between the electrode and electrochemical labels in the solution. By measuring the impedance change on the electrode surface, the quantification of H_2O_2 and cholesterol could be achieved. Based on the similar strategy, AgNPs could be employed for preparing AgNP-cysteine SAM through interactions between the silver surface and the carboxylate/amino groups of cysteine. The AgNP-modified electrode could be utilized for electro-catalysis of electroactive molecules [28].

As a commonly-used modification method, SAM is frequently combined with other modification methods to create multifunctional surface properties. A "linear layer-by-layer self-assembly" composite film was prepared by alternately depositing anionic tungstoborate ($BW_{12}O_{40}$) and cationic polyethylenimine (PEI)–Ag^+ complex. Under UV irradiation, Ag ions in ($BW_{12}O_{40}$/PEI–Ag^+)n multilayers were photochemically reduced into self-assembled Ag NPs. The obtained (BW_{12}/AgNPs)n films exhibited the electroreduction toward O_2 and long-lasting antibacterial properties [31]. Lin's group fabricated PtNP SAM respectively on the surface of graphitized carbon nanotubes and AuNPs to form nanocomposite. The PtNP SAM enhanced the electrocatalytic activity towards O_2 reduction and formic acid reactions, providing a facile approach to design high-performance fuel cells [32, 33]. Since 2008, graphene, a two-dimensional (2-D) sheet of carbon atoms in a hexagonal configuration with atoms, has proved to be an excellent nanomaterial for applications in electrochemistry due to its extraordinary electrical conductivity, large surface area and low cost [34]. Dong's group integrated graphene with NMNPs through SAM technology on the basis of electrostatic interactions between surface charge-changeable graphene nanosheets and NMNPs [35] to form multilayers of graphene/NMNP nanostructures. Moreover, they utilized cationic polyelectrolyte poly(diallyldimethyl ammonium chloride) (PDDA) functionalized graphene nanosheets as the building block in the self-assembly of graphene nanosheets/AuNPs heterostructure to enhance its electrochemical catalytic ability. The modification of PDDA altered the electrostatic charges of graphene, and made citrate-capped AuNPs more convenient to adsorb onto graphene surface. Compared with in situ synthesis of NMNPs on graphene [36–38], SAM provides an alternative strategy to obtain the graphene/NMNP hybrids with high-loading and uniform dispersion.

Layer-by-layer assembly

The layer-by-layer (LBL) assembly technique develops a complicated yet highly-ordered molecular architecture with precise control of the composition, number of layers and thickness of films at a molecular level [39]. The LBL assembly incorporates variety of matrixes with distinct nature, size and topology. Their property could be controlled by choosing different configurations, types of components and numbers of layers. With strong electron conductivity, adsorption ability as well as the biocompatibility, NMNPs have been commonly involved to form multilayer assembly on the electrode surface. Cho's group designed a multilayer structure based on catalase-encapsulated AuNPs which were electrostatically assembled with anionic and cationic polyelectrolytes [40]. This AuNP multilayer allowed electrostatic charge reversal and structural transformation through pH adjustment. Besides, it was capable of inducing high loading of catalase as well as effective electron transfer with the electrode. Moreover,

Luo's group developed a LBL route to prepare nanoporous Au film materials on electrode surface by alternately assembling AuNPs and AgNPs using 1,5-pentanedithiol as cross-linker. Through the mild dissolving of AgNPs at room temperature in $HAuCl_4$ solution, the generated nanoporous Au film possessed a uniform surface microenvironment and larger surface area [41]. Upadhyay et al. fabricated the multilayer of Au-Pt bimetallic alloy/glutaraldehyde/acetylcholinesterase (AChE)/choline oxidase (ChOx) on electrode surface. The combination of Au-Pt nanoparticles maintained the biological activity of enzymes, and showed excellent electrocatalytic properties for the detection of H_2O_2 [42].

As mentioned, variety of materials could be incorporated with NMNPs to form LBL structure, creating unique configurations and chemical properties. They include nanomaterials (e.g. single/multi-wall carbon nanotubes [43], SiO_2 nanospheres [44] and TiO_2 nanotubes [45]); polymers (polyaniline [46], phthalocyanine [47], polypyrrole [48], and chitosan [49]); biomolecules including DNA, enzymes and proteins [50]. For example, horseradish peroxidase (HRP) and glucose oxidase (GOx) could be embedded into the AgNP/carbon nanotubes/chitosan LBL film for the fabrication of glucose biosensor [51]. The bi-enzyme modified electrode exhibited fast and steady amperometric response for the electrocatalysis of HRP, which was correlated with GOx-based oxidation of glucose. Palmero et al. presented a LBL structure composed of polyaniline (PANI) and PtNPs. The number of PANI-PtNP layers and the nature of external layer determined its electrocatalytic performance for methanol oxidation [42]. More interestingly, the catalytic properties of PtNPs could be strengthened by changing the species of polymers in the LBL structure [41, 44].

Hybridization

To further enhance the conductivity, surface-to-volume ratio and biocompatibility of the electrode surface, the hybridization of NMNPs with single or multiple species of organic, inorganic nanomaterials and polymers has become one of the hottest modification strategies in recent years. Multi-dimensional carbon nanomaterials including graphene and single/multi-wall carbon nanotubes (SWCNTs/MWCNTs) have been considered as ideal material for hybridizing with NMNPs to fabricate electrochemical biosensors. For instance, Pt-CNT nanocomposite in which PtNPs were uniformly entrapped on CNT surface possessed large immobilizing area. In addition, they contained abundant oxygen-rich groups improving its solubility in water and biocompatibility for retaining the bioactivity of entrapped enzymes. Besides, the synergistic effect of PtNPs and CNTs significantly facilitated the H_2O_2-based catalysis on the electrode surface and lowered its overvoltage from 0.6 V to 0.02 V, which were of significance for the sensitive detection of H_2O_2 [52]. Similarly, the hybrid of graphene/AuNPs/chitosan nanocomposite is a suitable matrix for protein immobilization due to the participation of biocompatible AuNPs and chitosan, a polymer material with film forming and adhesion ability. The integration effect of graphene and AuNPs contributed to the excellent electrocatalytic activity toward H_2O_2 and O_2 [36].

Magnetic nano/micro-particles (e.g. Fe_3O_4) are another alternative materials frequently integrated with NMNPs in a broad range of biosensor applications, since they could be easily separated from bulk systems by an external magnetic field. This property not only enables the effective immobilization of biological molecules onto substrate surfaces, but also constructs the magnetically-controllable electrochemical detection systems. Since Fe_3O_4 nanoparticles were discovered to possess the intrinsic peroxidase-like activity [53], their application expanded from magnetic separation to direct electrochemical detection. By adding appropriate substrate (e.g. 3,3′,5,5′-tetramethylbenzidine (TMB), *o*-phenylenediamine (*o*-PD) [50] or N,N-diethyl-p-phenylenediamine sulfate (DPD) [54]), Fe_3O_4 nanoparticles could be used for measuring H_2O_2 through HRP-mimic catalysis and fabricating label-free biosensors [55]. However, the reactivity of Fe_3O_4 nanoparticles increases with the decrease of particle size, so they may undergo rapid degradation with relatively small size. To avoid this limitation, magnetic core–shell nanoparticles, in which Fe_3O_4 is the core and noble metal the shell, have been extensively proposed. These nanocomposites have better stability and biocompatibility which are attributed to the noble metal shell, meanwhile, maintain their magnetic property [56]. For instance, Fe_3O_4@Au NPs could be initially deposited onto electrode surface by applying a constant magnetic field, then conjugated with biological molecules such as enzymes and DNA onto the gold surface [57]. The large surface-to-volume ratio of Fe_3O_4@Au NPs makes them able to act as platforms where biological recognition events take place instead of on bulky electrode surface, providing a short diffusion distance for molecules and accelerating their mass transport [58]. After that, they could be easily concentrated onto substrate surface by external magnetic field and measured by electrochemical strategies [59, 60].

Sol-gel technology

The sol–gel process, in which inorganic precursors undergo various reactions resulting in the formation of a three-dimensional molecular network [61], has been widely used for the incorporation of different reagents in the development of biosensors. The combination of NMNPs with sol-gel which encapsulates nanoparticles within polymer matrices offers numerous advantages including preventing the oxidation and coalescence of NMNPs, remaining the stability of nanocomposite as well as facilitating the mass transport between nanomaterials and surroundings [62]. Furthermore, it provides

possibility of engineering nanoparticles with additional electrochemical, optical and mechanical properties. The properties of the sol–gel matrix and the stability of nanomaterial/sol-gel composite could be controlled by varying precursors, changing preparation conditions (pH, solvent, ratio of compounds, reaction time, etc.) as well as modifying NMNPs with functional groups, in order to keep the dispersion of nanoparticles in the sol-gel matrix. Different groups have reported that AuNPs, AgNPs [63] and their alloy [64] could be incorporated with three-dimensional porous silica network by chemical reduction or electro-deposition, and through the self-assembly of mercaptopropyltrimethoxysilane (MPS) or (3-mercaptopropyl)-trimethoxysilane (MPTS) in the sol-gel [65]. The NMNP-silica nanocomposite could be immobilized on the electrode surface for further modification of biological molecules. Besides, the NMNP-inorganic metal oxide sol-gel such as alumina could also be simply formed through dripping Al_2O_3 sol on the electrode followed by electrochemical deposition of NMNPs [66]. Moreover, Chen et al. proposed that the room-temperature ionic liquids (RTILs) could also be incorporated to synthesize AgNP/TiO_2 nanocomposite through sol-gel technology, and RTILs worked as the dispersers and stabilizers to control the growth of AgNPs on TiO_2 surface and keep the dispersion of Ag clusters [67].

Direct electrochemistry of proteins on NMNP-modified electrode surface

Electron transfer in redox proteins plays a key role in many biological reactions such as respiration and photosynthesis, and the direct electron transfer of proteins is of great interest for bioelectrocatalysis. However, most of redox enzymes and proteins, such as glucose oxidase (GOx), horseradish peroxidase (HRP) and hemoglobin (Hb)/myoglobin (Mb) lack direct electrical communications with electrode surfaces due to deeply-buried redox centers insulated by the protein shells, or the redox centers are too far away from electrode surface to perform direct electron transfer. The utilization of NMNPs has been proposed to overcome this problem by employing nanoparticles as connecters to provide an electron relay pathway from the redox center regions to electrode surface. In addition, NMNPs provides a microenvironment which makes proteins more free in their orientation, thereby reducing the insulating effect of the protein shells.

Researchers have studied the direct electrochemistry of different proteins/enzymes and fabricated respective biosensors. Table 1 lists some of the recent advances in the direct electron transfer (DET) study of redox proteins. Single or multiple kinds of NMNPs are integrated with inorganic/organic nanostructures to form highly-organized composite, and the facile surface modification of NMNPs provides different (e.g. carboxyl and amino) functional groups for the further immobilization of proteins. Zhang et al. utilized pulse electro-deposition to obtain uniform and dispersed AuNPs on the surface of TiO_2 nanotube arrays. The incorporation of TiO_2 and AuNPs significantly enhanced the surface areas on the electrode, followed by covalent immobilization of GOx onto AuNP surface through 1-ethyl-3-[3-dimethylaminopropyl] carbodiimide hydrochloride (EDC) and N-hydroxysuccinimide (NHS) coupling reaction to construct enzyme monolayer [68]. Alternatively, the enzyme immobilization could be accomplished by proton-conductive polymers such as nafion and chitosan, which possess high permeability toward water, good adhesion and biocompatibility. Luan et al. co-immobilized graphene and HRP into chitosan, followed by electro-deposition of AuNPs on the surface [69]. The fabricated AuNP/graphene/HRP/chitosan worked as "molecular wires" to achieve the direct electrochemistry of HRP, and exhibited sensitive detection of H_2O_2 with a limit of 1.7×10^{-6} M. Instead of using organic nanostructures, the flowerlike zinc oxide (ZnO) nanoparticles could also be hybridized with AuNPs and nafion film to form nanocomposite [70], so that the entrapped HRP undergone a direct surface-controlled quasi-reversible electrochemical reaction, with the electron transfer rate constant (ks) of 1.94 s^{-1}.

To further obtain a better control with the orientation as well as the appropriate alignment of the redox center of proteins on the electrode surface, different groups have explored the attachment of single NMNP as nanowire to the redox center of proteins. The first achievement was the surface reconstitution of apo-GOx on an AuNP-functionalized flavin adenine dinucleotide (AuNP-FAD)-monolayer electrode. AuNP with the appropriate dimension and functionalization adjacent to the enzyme redox center acted as a current collector to the electrode surface, which made the reconstituted GOx exceed the electron transfer features of native enzyme [92]. Recently, Schiffrin's group further demonstrated the specific recognition between the metallic redox center of proteins and NMNPs by reporting the direct electrical connection of the metal center of Galactose oxidase (GOase) by chemical coordination to a linker attached to single AuNP, which acted as an electron relay [71] (Fig. 1a). GOase contained three domains and a single copper active site (cavity size) lying close to the protein surface. The connection between Cu center and single AuNP was based on the introduction of thioctic acid monolayer-capped AuNP with suitable size inside the copper pocket of GOase to achieve direct coordination with the metal center. Thioctic acid-protected AuNP was linked to a biphenyl dithiol-SAM modified electrode and then GOase was immobilized by coordination to the carboxylate-functionalized AuNP (Fig. 1b). By employing hybrid nanowire, one AuNP was coupled with one copper metal site region, and the involvement of AuNP facilitated the direct electron transfer between the enzyme and electrode surface. A well-defined DET of GOase could be observed, shown by the clear

Table 1 Direct electrochemistry of proteins on NMNP-modified electrode surface

Protein	NMNPs	Immobilization Mode	Analyte	Performance	References
Cytochrome c	AuNPs/ AgNPs	Layer-by-layer (LBL) assembly of AuNPs and AgNPs through 1,5-pentanedithiol as cross-linker	H_2O_2	Electron transfer rate constant (ks)=3.9 s^{-1}; limit of detection (LOD)=6.3×10^{-6} M; Linear detection range (LDR)=1×10^{-5}~1.2×10^{-3} M	[41]
galactose oxidase (GOase)	AuNPs	Direct electrical wiring of the metal center of GOase by coordination of a linker attached to single gold nanoparticle	Galactose	ks=0.6 s^{-1}; K_m^{app}=0.175 M;	[71]
glucose oxidase (GOx)	AuNPs	Hybridization of multi-wall carbon nanotubes (MWCNTs) and nanostructured SnO_2-AuNPs	Glucose	LOD=4×10^{-3}~2.4×10^{-2} M in human blood samples	[72]
GOx	AuNPs	Hybridization of AuNPs and TiO_2 nanotube arrays	Glucose	ks=0.262 s^{-1}; K_m^{app}=7.2×10^{-3} M; LOD=3.1×10^{-4} M (S/N=3); LDR=4×10^{-4}~8×10^{-3} M	[68]
GOx	PtNPs	Hybridization of PtNPs and clay clusters encapsulated with poly(amidoamine) dendrimer	Glucose	LOD=4×10^{-6} M (S/N=3); LDR=1×10^{-5}~1.6×10^{-2} M	[73]
GOx	AuNPs	Hybridization of Fe_3O_4, AuNPs and chitosan	Glucose	LOD=1.2×10^{-6} M (S/N=3); LDR=3×10^{-6}~5.7×10^{-4} M	[74]
GOx	AuNPs	Hybridization of chitosan, graphene and AuNPs	Glucose/H_2O_2	Sensitivity of H_2O_2=99.5 μAmM^{-1} cm^{-2}; LDR of H_2O_2=2×10^{-4}~4.2×10^{-3} M; LOD of glucose=1.8×10^{-4} M; LDR of glucose=2×10^{-3}~1.4×10^{-2} M	[36]
GOx	AuNPs	Tetraethoxysilane sol-gel encapsulated by AuNPs and graphite powder	Glucose	LOD=1.3×10^{-3} M; LDR=5×10^{-4}~5.5×10^{-2} M	[75]
Hemoglobin (Hb)	AuNPs	Hybridization of chitosan and AuNPs/3-aminopropyl triethylene silane/ prussian blue (PB) nanocomposite	H_2O_2	LOD=1×10^{-7} M (S/N=3); LDR=2×10^{-6}~2.8×10^{-4} M	[49]
Hb	AuNPs	Core-shell Fe_3O_4@Au nanoparticles	H_2O_2/ trichloroacetic acid (TCA)	LOD of H_2O_2=6.7×10^{-7} M (S/N=3); LDR of H_2O_2=3.4×10^{-6}~4×10^{-3} M; LOD of TCA=1×10^{-6} M (S/N=3); LDR of TCA=1.6×10^{-6}~4.8×10^{-3} M	[76, 77]
Hb	AuNPs	LBL assembly of positively-charged AuNPs and MWCNTs	H_2O_2	LOD=9.6×10^{-7} M (S/N=3); LDR=3.6×10^{-6}~3×10^{-3} M	[78]
Hb	AuNPs	LBL assembly of AuNPs and colloidal carbon sphere core covered by porous silica shell (C@SiO_2)	H_2O_2	K_m^{app}=7.149×10^{-5} M; LOD=8×10^{-8} M (S/N=3); LDR=5×10^{-6}~8×10^{-5} M	[79]
Hb	PtNPs	PtNP-enhanced poly(chloromethyl thiirane) cross-linked chitosan hybrid film	H_2O_2	K_m^{app}=2.136×10^{-5} M; LOD=2.8×10^{-8} M (S/N=3); LDR=4.4×10^{-7}~4.4×10^{-5} M	[80]
Hb	AuNPs	Three-dimensionally ordered macroporous AuNP-doped TiO_2 film	H_2O_2	ks=1.12 s^{-1}; LOD=6×10^{-7} M; LDR=5×10^{-6}~1×10^{-3} M	[81]
Hb	PtNPs	Hybridization of graphene and PtNPs	H_2O_2	K_m^{app}=5.4×10^{-4} M; LOD=1×10^{-6} M (S/N=3); LDR=1×10^{-5}~1×10^{-3} M	[37]
Hb	AgNPs	Self-support of AgNPs on $Ag_2V_4O_{11}$ nanobelts	H_2O_2	ks=2.6 s^{-1}; LOD=3×10^{-7} M; LDR=1×10^{-6}~1.2×10^{-4} M	[82]
Horseradish peroxidase (HRP)	AuNPs	Hybridization of graphene/HRP/chitosan/AuNPs	H_2O_2	K_m^{app}=2.61×10^{-3} M; LOD=1.7×10^{-6} M (S/N=3); LDR=5×10^{-6}~5.13×10^{-3} M	[69]
HRP	AuNPs	Flowerlike ZnO/AuNPs/Nafion	H_2O_2	K_m^{app}=1.76×10^{-6} M; LOD=9×10^{-6} M (S/N=3); LDR=1.5×10^{-5}~1.1×10^{-3} M	[70]
HRP	AuNPs	LBL assembly of calcium carbonate/AuNPs	H_2O_2	LOD=1×10^{-7} M (S/N=3); LDR=5×10^{-7}~5.2×10^{-3} M	[83]
HRP	PtNPs	Hybridization of electro-copolymerizated of PtNPs/poly(neutral red)/MWCNTs	H_2O_2	ks=1.83 s^{-1}; LOD=1.1×10^{-6} M; LDR=3.6×10^{-6}~4.3×10^{-3} M	[84]

Table 1 (continued)

Protein	NMNPs	Immobilization Mode	Analyte	Performance	References
HRP	AuNPs	Self-assembly monolayer (SAM) of AuNPs and poly(diallyldimethylammonium chloride)	H_2O_2	$K_m^{app}=6.9\times10^{-4}$ M; LOD=9.9×10^{-5} M (S/N=3); LDR=1.96×10^{-4}~9.09×10^{-4} M	[85]
HRP	AuNPs	Hybridization of electropolymerizad AuNPs with 2-mercaptoethanesulfonic acid, 3-mercaptophenyl boronic acid or p-aminothiophenol	H_2O_2	$K_m^{app}=1.01\times10^{-3}$ M; LOD=1.5×10^{-6} M; LDR=5×10^{-6}~1.1×10^{-3} M	[86]
HRP	AuNPs/PtNPs	Hybridization of AuNPs/chitosan/HRP/ electrodeposited PtNPs/polyaniline (PANI) nanofibers	H_2O_2	$K_m^{app}=1.9\times10^{-3}$ M; LOD=2.8×10^{-6} M (S/N=3); LDR=7×10^{-6}~1.4×10^{-2} M	[87]
HRP, GOx	AuNPs	Silica sol-gel and AuNPs	Glucose	LOD of GOx mono-enzyme sensor=2×10^{-5} M, LDR=5×10^{-5}~4×10^{-3} M; LOD of HRP-GOx bi-enzyme sensor=1×10^{-5} M; LDR=2×10^{-5}~3.2×10^{-3} M	[88]
HRP, Hb, myoglobin (Mb)	AuNPs	Hybridization of AuNPs and bacterial cellulose nanofibers	H_2O_2	LOD=1×10^{-7} M (S/N=3); LDR=3×10^{-7}~1×10^{-3} M in the presence of the mediator hydroquinone (HQ)	[89]
Mb	AuNPs	Hybridization of AuNPs and MWCNTs	H_2O_2	LOD=6×10^{-7} M; LDR=2×10^{-6}~5×10^{-4} M	[90]
Mb	AuNPs	Hybridization of AuNPs, Mb and Nafion film	H_2O_2	ks=0.6 s^{-1}; LDR=1×10^{-5}~2.35×10^{-4} M	[91]

Abbreviations: *GOase* galactose oxidase, *GOx* glucose oxidase, *Hb* hemoglobin, *HQ* hydroquinone, *HRP* horseradish peroxidase, *LBL* layer-by-layer, *LDR* linear detection range, *LOD* limit of detection, *Mb* myoglobin, *MWCNT* multi-wall carbon nanotube, *ks* electron transfer rate constant, K_m^{app} apparent Michaelis-Menton constant, *PANI* polyaniline, *PB* prussian blue, *SAM*: self-assembly monolayer, *S/N* signal-to-noise ratio, *TCA* trichloroacetic acid, TiO_2 titanium dioxide

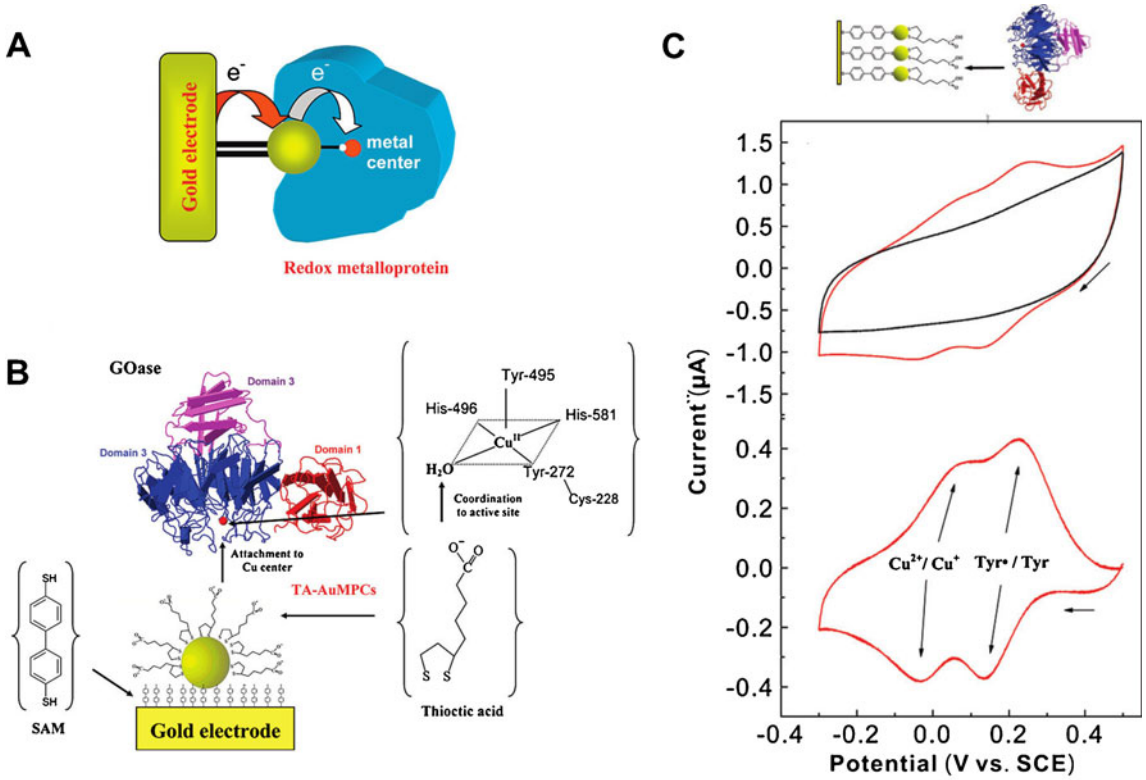

Fig. 1 Direct electron wiring of the metal center of metalloenzyme GOase linking to single AuNP. **a**) Schematic description of enzyme-single AuNP linkage. **b**) Structure of GOase and reaction strategy for immobilizing GOase onto gold electrode. **c**) Cyclic voltammograms (CVs) of a gold electrode modified with a SAM consisting of biphenyl-4,4′-dithiol and carboxylate-AuNP before (background, *black line* in the top figure), after incubation into GOase protein solution (*red line* in the top figure); and the processed CV after background voltammogram subtraction (*red line* in the bottom figure). Measurements were performed in nitrogen-saturated 20 mM 2-(*N*-morpholino)ethanesulfonic acid (MES) buffer, pH 7.5. Scan rate: 20 $mV \cdot s^{-1}$. (Adapted with permission from ref. [71]. Copyright 2009 American Chemical Society)

appearance of two voltammetric peaks, which were ascribed respectively to the oxidation/reduction of tyrosyl radical (Tyr•272) and Cu^{II}/Cu^{I} redox couple (Fig. 1c).

NMNP-based signal amplification strategies for the fabrication of bioaffinity sensors

Bioaffinity sensors are based on biological recognition events in which target molecules are involved. Depending on the nature of biorecognition (e.g. immune reaction; ligand-receptor interaction and DNA hybridization), they could further be classified into different subtypes, including immunosensors; nucleic acid sensors, small organic/inorganic molecule sensors etc. Different from facilitating electron transfer in the fabrication of redox protein sensors, NMNPs provide great promise as versatile labels and signal amplifiers in bioaffinity assays. On the basis of biological recognition element and signal-transduction element working as the main components of a biosensor, the functions of NMNPs could respectively be ascribed as 1) carriers of biological molecules for the recognition events; 2) tags for electrochemical signal response, amplification and output. The facile modification of functional groups on the NMNP surface makes them capable of loading single or multiple species of biological molecules. Moreover, the optimization and quantification of functional groups/ligands on NMNP surface could be easily achieved by tuning the size, shape and surface of NMNPs. All these functionalization of NMNPs improves the performance of bioaffinity sensors in the aspects of remarkable sensitivity, specificity and biocompatibility. To date, three approaches have been developed for signal amplification in NMNP-based bioaffinity sensors.

(1) NMNPs are directly used as electroactive labels to amplify the electrochemical response. In the presence of target, NMNPs could be specifically coupled to the modified electrode surface due to the recognition event. Correspondingly, the acidic oxidation NMNPs into ions which could easily measured by electrochemical strategies would be correlated with target concentration. Chen's group developed an aggregated AgNP tag by DNA hybridization (Fig. 2) [93]. The initial AgNP seeds conjugated with both oligo(d)A and probe DNA strands were hybridized with AgNPs which were conjugated

with oligo(d)T to form a large cluster of AgNPs (Fig. 2a). After that, the Ag aggregate was anchored onto electrode surface through the hybridization between probe DNA and the targets (Fig. 2b). The generated Ag aggregate had an averaged diameter of 410 nm (Fig. 2c) and showed 10^3-fold amplification in oxidation currents compared with AgNP seeds (20 nm diameter) using differential pulse voltammetry (DPV). Therefore, this biosensor achieved a detection limit of 5×10^{-18} M target molecules (about 120 molecules in 40 μL of sample soluiton) as well as a broad detection range from 1×10^{-17} M to 1×10^{-13} M (Fig. 2d). In addition, this strategy was applicable to multiplexed DNA target measurements utilizing array chips, achieving the simultaneous detection of four DNA targets. Alternatively, they also synthesized a nano-cluster which was composed of Fe_3O_4 nanoparticle core and the alternate coatings of polystyrene sulfonate sodium salt (PSS), poly(diallyldimethylammonium chloride) (PDDA) and AuNPs *via* electrostatic LBL assembly for the detection of DNA hybridization. The polymer coating significantly enlarged the surface area of nano-cluster, resulting in more absorption of AuNPs. In the presence of target DNA, the nano-cluster was linked onto electrode surface, followed by catalytic deposition of silver to form a thick shell on nano-cluster surface. By immersing the nano-cluster modified electrode into the presence of HNO_3 electrolyte solution and measuring the released Ag^+ ions, the detection limit was down to 1×10^{-16} M, 800 times lower than that only using AuNPs as labels [94]. Instead of linking NMNPs onto the electrode surface by biological interactions, NMNPs could also be directly immobilized by enzymatic reactions, in order to

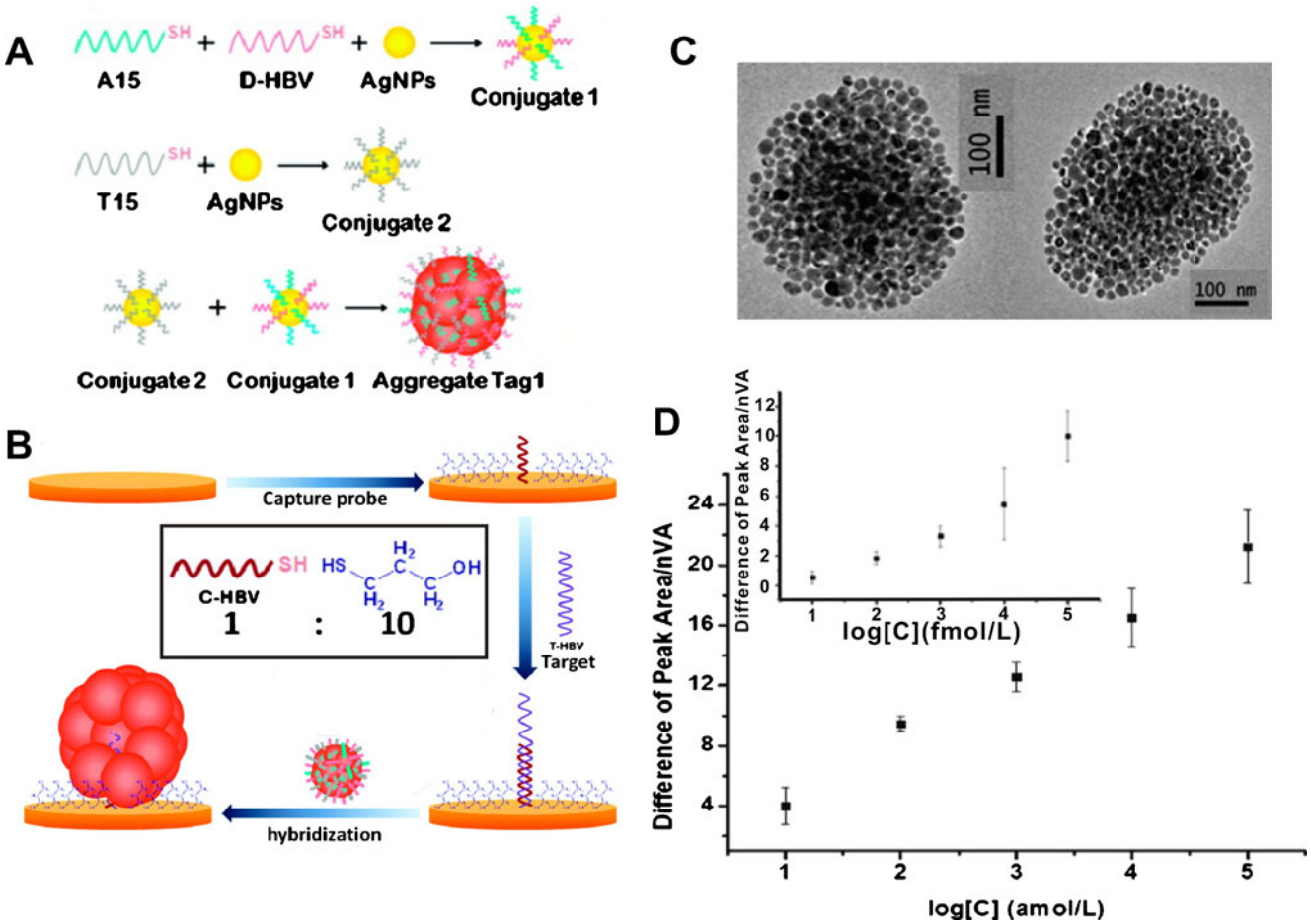

Fig. 2 Schematic description of Ag aggregate-based signal amplification for the detection of DNA hybridization (Target: DNA sequence from Hepatitis B virus, HBV). **a**) The preparation of Ag aggregate utilizing the hybridization of Conjugate 1 (oligo(d)A (A15)/probe DNA strand (D-HBV)-labeled AgNP seeds) and Conjugate 2 (oligo (d)T (T15)-labeled AgNP seeds). **b**) Fabrication of electrochemical assay and detection process. **c**) Scanning electron microscopy (SEM) images of Ag aggregate. D) Linear calibration curves of DNA targets in the range from 1×10^{-17} M to 1×10^{-13} M based on the signal amplification of Ag aggregate; inset is the control in the range from 1×10^{-14} to 1×10^{-10} M using AgNP seeds. (Adapted with permission from ref. [93]. Copyright 2010 American Chemical Society)

generate enhanced electrochemical signals. Lai et al. functionalized AuNPs with alkaline phosphatase-labeled antibody (ALP-Ab) to identify target antigen. After sandwich-type immunoreaction, the AuNPs loaded with ALP-Abs were captured by the antibodies covalently modified on the electrode surface. The involvement of AuNPs and ALP enzyme catalyzed the hydrolysis of 3-indoxyl phosphate (3-IP) and resulted in the reduction of Ag^+ ions to AgNPs. The deposited AgNPs could easily be quantified by anodic stripping analysis and correlated with the concentration of target antigen [95].

(2) NMNPs act as carriers to load large number of electroactive labels through covalent linkage or electrostatic interaction, which directly generate quantitive electrochemical signals. Frequently used electrochemical tags include ferrocene [96], methylene blue [97], tris(bipyridine)ruthenium(II) chloride [98], pentaamminechlororuthenium(III) chloride [99], 2-mercapto-1-methyl imidazole [100], thionine [101] and electroactive drug molecules such as doxorubicin [102]. The electrochemical signal generated by the enrichment of these labels corresponds with the amount of target molecules captured *via* the biorecognition events happening on the electrode interface. Based on this strategy, researchers have designed various "signal-on" electrochemical sensors. In contrast, "signal-off" sensors using redox labels such as $[Fe(CN)_6]^{3-/4-}$ rely on the impedance effect of NMNPs and the electron repulsion force between labels and negative-charged NMNPs. As a result, the number of NMNPs on the electrode surface, which is determined by the concentration of target molecules, is inversely correlated with generated electrochemical signals [103]. To further enhance the impedance effect, the NMNP surface could be coated by polymers with the same charge as electrochemical labels. The size of NMNPs was enlarged, meanwhile the repulsion between the NMNPs and the labels was strengthened, both of which contributed to the "signal amplification" effect [104].

Recently, the quantum dots hybridized with NMNPs have become another effective tag to generate electrochemical signal and exhibit amplification. For example, carboxyl group-functionalized cadmium sulfide nanoparticles (CdS NPs) could be conjugated with amino group-modified AuNPs to form nanocomposite, and the signal output is accomplished by measuring cadmium ions dissolved from CdS NPs in acidic solution [104]. Chen's group further explored the electrochemical functions of quantum dots to fabricate an electrochemiluminescent (ECL) biosensor by measuring the nanoscale-localized energy transfer between the excitons in the CdS NPs and the plasmons in the AuNPs [105]. Single-stranded DNA (ssDNA)-labeled CdS NPs were immobilized on the electrode surface, and then AuNPs conjugated with complementary DNA strands which also identified target protein were hybridized with CdS NPs with a separation length of ca. 12 nm. The ECL emission from CdS NPs induced the surface plasmon resonance (SPR) of Au NPs, and the SPR in turn lead to 5-fold enhancement of the ECL response of CdS NPs. In the presence of target, the higher affinity between the protein and DNA strands resulted in the de-hybridization of duplex and release of AuNPs from CdS NPs. Subsequently, the ECL intensity was strongly decreased. Compared with using electroactive labels, the energy transfer between NMNPs and semiconductor quantum dots provided dual signal amplification, making the detection limit of target protein down to 1×10^{-16} M.

(3) Enzyme-functionalized NMNPs are employed as labels to enhance the detection sensitivity by measuring the enzymatic catalysis of electroactive substrates on the electrode surface. HRP, GOx and ALP have been considered as the suitable enzymes for signal enhancement, since they are easy to conjugate with other biological molecules and co-immobilize onto NMNP surface with large quantity and good stability. Ju's group constructed a tracer label, which was composed of cationic polyelectrolyte polymer-coated CNTs uniformly attached with negatively-charged AuNPs through electrostatic interaction [106] (Fig. 3). The combination of CNTs and AuNPs greatly enhanced the surface-to-volume ratio of the tracer label; and the biocompatibility of AuNPs facilitated the further conjugation of GOx and antibody onto the tracer label (Fig. 3a). To obtain electrochemical output signal, the substrate electrode was constructed by coating LBL of colloidal prussian blue (PB), AuNPs and capture antibody (Fig. 3b). In the presence of target antigen, the tracer label was captured onto the electrode surface, and PB immobilized on the electrode surface acted as a mediator to catalyze the reduction of H_2O_2 produced in the GOx-based enzymatic reaction (Fig. 3c). The triple signal amplification was attributed to GOx-functionalized tracer labels combining AuNPs and CNTs, as well as the electron transfer between enzymatic reaction and PB-based electrocatalysis. The enzyme-based signal amplification strategy could be extended to the fabrication of versatile biosensors, depending on the recognition elements modified on the electrode and NMNP surface [107, 108]. Li's group designed a biosensor to monitor phosphorylation by making self-assembly layer of peptides on gold electrode surface. The peptides were then phosphorylated by protein kinase and recognized by specific biotin-labeled antibody. The Au-NPs carrying HRP-conjugated streptavidin worked as signal amplifier and were immobilized onto electrode surface through

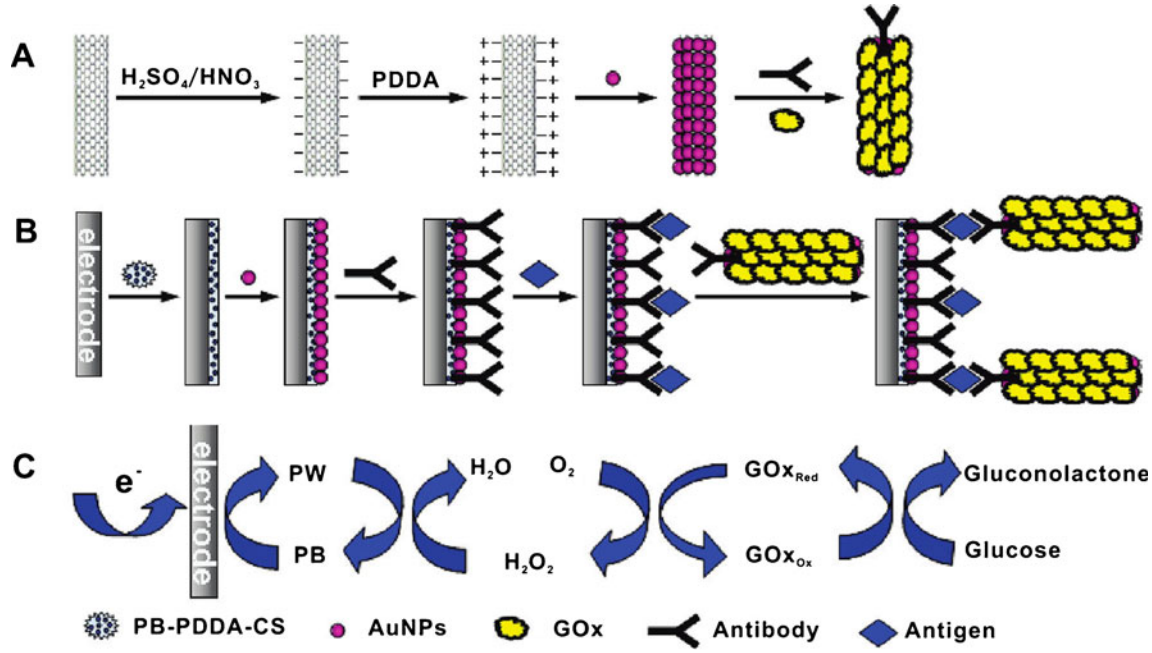

Fig. 3 **a**) Preparation of glucose oxidase (GOx)-functionalized tracer labels. The poly(diallyldimethylammonium chloride) (PDDA)-coated carbon nanotubes (CNTs) were electrostatically conjugated with AuNPs, followed by the adsorption of GOx and antibody. **b**) Functionalization of electrode surface using the composite of prussian blue (PB)/PDDA/chitosan (CS)/AuNPs and the sandwich-type immunoreaction happening on electrode surface. **c**) Electrochemical response mechanism induced by the enzymatic reaction. (Adapted with permission from ref. [106]. Copyright 2009 American Chemical Society)

biotin–avidin interaction. Through enzymatic oxidation of substrate 3,3′,5,5′-tetramethylbenzidine (TMB), the generated electrochemical signals could be utilized to evaluate phosphorylation [109].

Genesensors

Genetic analysis plays crucial role in a wide range of research fields including diagnostics of genetic diseases, monitoring of infectious bacteria and pathogen, as well as screening of environmental hazards and biological warfare agents. Meanwhile, it is always of great concern to determine the gene sequences in living organisms and other complex systems. Although plenty of DNA/RNA microarrays are commercially available nowadays, it is still worthwhile to design novel genesensors with inherent sensitivity, efficiency and cost benefits, which is also the reason that electrochemical genesensors have received tremendous research interest in recent years (Table 2). The working principle of a typical DNA hybridization sensor is fairly simple: The probe DNA strands are firstly immobilized onto electrode surface. With the addition of complementary target DNA strands, the hybridization process could be transduced into electrochemical signal, either from hybridization-induced physical enrichment of electroactive labels which are either covalently or noncovalently (*via* intercalation) attached to DNAs, or from the oxidation of bases in DNA strands. Nevetheless, some drawbacks still exist: the covalent linkage of electroactive labels onto DNA strands is complicated or time-consuming, and the number of labels is limited. If the signal was generated by the redox of bases, the lifetime of genesensors could be restricted due to irreversible oxidation. The unique physical, chemical and electrochemical properties of NMNPs make them promising to resolve the potential limitations of traditional genesensors and improve their performance. The large surface-to-volume ratio and biocompatibility of NMNPs facilitate the effective immobilization of DNA probes and accelerate the electron transfer between DNA bases and electrode surface. More importantly, it provides more opportunities for electrochemical signal transduction and amplification.

Direct oxidation of bases in DNA helix is the first and most straightforward strategy of DNA detection on electrode surface. It is simple and requires no external modifications of DNA. However, the direct electrochemistry of bases has been limited due to their high over-potentials and limited voltammetric peaks. Only the oxidation of guanine (oxidation peak at 1.0~1.1 V vs Ag/AgCl) is frequently employed as electroactive probe for the fabrication of genesensors. Qian et al. encapsulated gold-palladium (Pd) alloy with dendrimer poly(amidoamine) (PAMAM) into the chitosan composite to immobilize DNA. The Au-Pd bimetallic nanoparticles enhanced the electron transfer between DNA

Table 2 NMNP-based genesensors

Targets	NMNPs	Electrode Modification	Electrochemical Labels for Signal Output and Amplification	Detection Approach	Performance	References
Evaluation of DNA damage and antioxidant activity of sericin	AuNPs/ PdNPs	Double-stranded DNA/poly (amidoamine) dendrimer/AuNPs/PdNPs/chitosan	oxidation of guanine	CV	Sericin showed effective antioxidant activity at the concentration of 0.05~0.90 $g{\cdot}L^{-1}$	[110]
DNA hybridization	AgNPs	Probe DNA/AgNPs/poly(trans-3-(3-pyridyl) acrylic acid) (PPAA)/ MWCNTs	DNA duplex intercalator adriamycin	DPV	LOD=3.2×10^{-12} M, LDR=9×10^{-12}~9×10^{-9} M	[111]
DNA hybridization	AuNPs	biotin-labeled probe DNA/ streptavidin-coated AuNPs	luminol-AuNPs labeled 2^{nd} probe DNA	ECL	LOD=1.9×10^{-16} M, LDR=3.1×10^{-15}~3.1×10^{-11} M	[112]
DNA hybridization	AuNPs/ AgNPs	SAM of probe DNA	nanocomposite of Fe_3O_4/polystyrene sulfonate sodium (PSS)/poly (diallyldimethylammonium chloride) (PDDA)/AuNPs/2^{nd} probe DNA followed by AgNP enhancement	ASV	LOD=1×10^{-16} M, LDR=1×10^{-16}~1×10^{-14} M	[94]
Gene fragments isolated from *Bacillus anthracis*	AuNPs	SAM of probe DNA	AuNPs conjugated with thiol-ended 2^{nd} probe sequences	QCM	LOD of *Bacillus anthracis*=3.5×10^{2} $CFU{\cdot}mL^{-1}$, LDR=3.5×10^{2}~3.5×10^{7} $CFU{\cdot}mL^{-1}$	[113]
Gene fragments isolated from H5N1 bird flu virus	AgNPs	SAM of neutral peptide nucleic acid (PNA)	amine-functionalized positively charged AgNPs	CV	LOD=1×10^{-15} M; LDR=1×10^{-14}~1×10^{-9} M	[114]
Gene fragments isolated from Hepatitis B virus (HBV)	AgNPs	SAM of probe DNA	Ag aggregates formed through the hybridization between complementary ssDNA on AgNPs	DPV	LOD of HBV=1×10^{-18} M, LDR=1×10^{-17}~1×10^{-13} M	[93]
Hepatitis C Virus RNA	AuNPs	probe DNA/AuNPs	thionine	DPV	LOD=3.1×10^{-22} M, LDR=1×10^{-21}~1×10^{-10} M	[101]
Point mutation detection based on surface ligation reaction by *Escherichia coli* DNA ligase	AuNPs	SAM of probe DNA	AuNPs conjugated with target sequences and $[Ru(NH_3)_6]^{3+}$	chronocoulometry	LOD=9×10^{-13} M; LDR=1×10^{-12}~1×10^{-9} M	[115]
Single and double-base mismatch	AuNPs	AuNPs/electrochemically reduced graphene oxide	oxidation of bases	DPV	simultaneous detection of four DNA bases and discrimination of single and double-base mismatches	[116]
Single-base mismatch	PtNPs	SAM of probe DNA	PtNPs conjugated with thiol-ended 2^{nd} probe sequences	CV and DPV	CA, GA, GT, and TT mismatches	[100]
Single-base mismatch	AgNPs	SAM of probe DNA/3-mercaptopropionic acid (MPA)	AgNPs conjugated with thiol-ended 2^{nd} probe sequences	EIS and DPV	Detection of CA, GA, GT, and TT mismatches at near and far positions of duplex	[117]
Single nucleotide polymorphism (SNP)	AuNPs	AuNPs/probe DNA	hydrazine oxidation enhanced by $NaBH_4$ treatment	LSV	LOD=1×10^{-15} M, LDR=1×10^{-15}~1×10^{-11} M	[118]
SNP	AuNPs	probe DNA/AuNPs/mesoporous silica/graphene	ferrocene	DPV	LOD=1×10^{-14} M, LDR=1×10^{-14}~1×10^{-10} M	[119]

Abbreviation: *ASV* anodic stripping voltammetry, *CV* cyclic voltammetry, *DPV* differential pulse voltammetry, *ECL* electrochemiluminescence, *EIS* electrochemical impedance spectroscopy, *LDR* linear detection range, *LOD* limit of detection, *LSV* linear sweep voltammetry, *MPA* 3-mercaptopropionic acid, *MWCNTs* multi-wall carbon nanotubes, *PDDA* poly(diallyldimethylammonium chloride), *PNA* peptide nucleic acid, *PPAA* poly(trans-3-(3-pyridyl) acrylic acid, *PSS* polystyrene sulfonate sodium, *QCM* quartz crystal microbalance, *SAM* self-assembly monolayer, *SNP* single nucleotide polymorphism

and electrode surface to exhibit enlarged oxidation signal. Since the Fenton-type reaction (H_2O_2 and iron catalyst) could induce the generation of hydroxyl radical (·OH) and lesions in DNA, the oxidation of guanine was also able to monitor the DNA damage and evaluate the protective activity of antioxidants [110]. Jiao's group integrated NMNPs with electrochemically-reduced graphene oxide (ERGNO) film, which possessed high electrical conductivity and synergistic electrocatalytic activity, to accomplish the simultaneous detection of four DNA bases (G, T, C, A) (Fig. 4) [116]. The function of AuNP/ERGNO film was to enhance the peak currents of bases and shifted the anodic potential negatively, which avoided their overlay and achieved the simultaneous detection of four bases (Fig. 4a). Even when the ssDNA sequences were immobilized on the electrode surface, the potential responses of four bases were very similar with the value obtained using single base solutions. Because the current responses of bases coincided precisely with the base content of each sequence at the electrode surface, this strategy was able to discriminate single-base and double-base mismatches, without DNA hybridization or any electrochemical labeling (Fig. 4b).

Due to the incorporation of NMNPs, the significant improvement in the detection sensitivity of DNA hybridization has driven electrochemical genesensors to apply in widespread areas, including DNA damage, DNA-drug interactions, point mutationand bacteria/virus screening [120]. For instance, Hepatitis C virus (HCV) is a RNA virus which displays extensive genetic heterogeneity and the major cause of chronic hepatitis and progressive liver fibrosis [121]. To detect the HCV at RNA level and identify the HCV genetype, an ultrasensitive electrochemical approach was developed, combining the site-specific cleavage of *Bam*HI endonuclease and signal amplification of AuNPs [101]. The probe DNA was initially immobilized onto the electrode surface, and then conjugated with thionine-labeled AuNPs in the end. After its hybridization with 244 bp HCV cDNA target, the *Bam*HI endonuclease was added to cleave the duplex, leading to the release of duplex-linked AuNPs and correspondingly strong decrease of electrochemical signal generated by thionine. Since the target cDNA was obtained through Reverse Transcription Polymerase Chain Reaction (RT-PCR) from RNA virus, and also attributed to the amplification of thionine-conjugated AuNPs, the detection limit

A

DNA base	DPV signal	AuNPs/ERGNO/GCE	DNA sequence at AuNPs/ERGNO/GCE
G	I_{ox} 10^{-5}A	1.585	
	E_{ox} V	0.620	0.644
A	I_{ox} 10^{-5}A	1.111	
	E_{ox} V	0.932	0.968
T	I_{ox} 10^{-7}A	7.431	
	E_{ox} V	1.098	1.136
C	I_{ox} 10^{-5}A	2.219	
	E_{ox} V	1.264	1.372

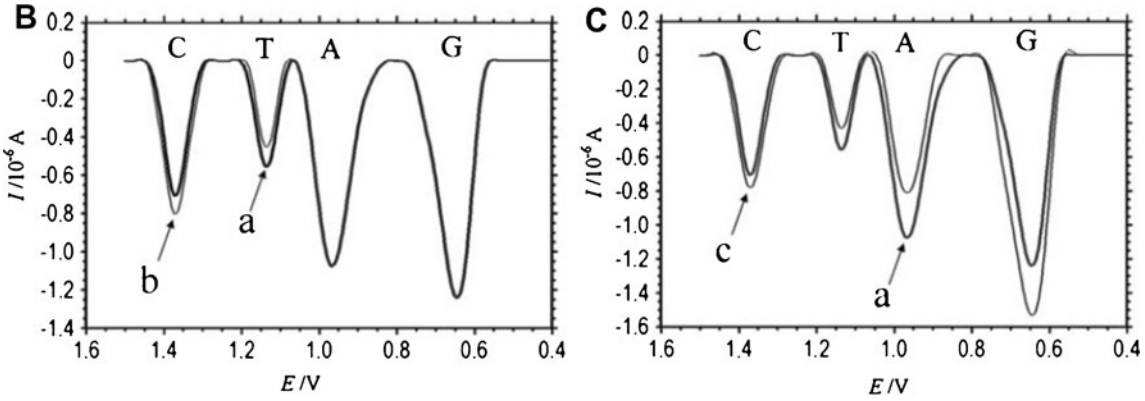

Fig. 4 **a**) Electrochemical responses (I_{ox}: oxidation peak currents; E_{ox}: oxidation peak potentials) for G, A, T, C and DNA sequence (*5′-ACT ACC TTT GC-3′*) at AuNP/ERGNO-modified glassy carbon electrode (GCE) surface in Britton–Robinson buffer, pH 7.0. Concentrations of bases G, A, T, C=1×10^{-4} M; concentration of DNA sequence=1×10^{-6} M. B) and C) Baseline-corrected DPVs at AuNPs/ERGNO/GCE for (**a**) DNA sequence, (**b**) single-base mismatched DNA sequence (*5′-ACT ACC CTT GC-3′*) and (**c**) two-base mismatched DNA sequence (*5′-GCT ACC CTT GC-3′*). Concentrations of different sequences=1×

was as low as 3.1×10^{-22} M, approximately 10^5 lower than the control without the involvement of AuNPs. The obtained detection linear range was from 1×10^{-21} to 1×10^{-10} M, which was one of the broadest in reported literatures.

As a negatively charged biopolymer, DNA can bind to any positively charged molecules and ions, which makes it challenging to achieve high selectivity for biosensor design. Since 2004 it was found that mercury ions (Hg^{2+}) possess the property of binding specifically to two DNA thymine bases (T) and promoting T–T mismatches to form stable base pairs, genesensors are becoming a good choice for the detection of metal ions [122]. For example, the probe DNA containing multiple T-bases for Hg^{2+} binding was immobilized onto electrode surface. In the presence of Hg^{2+}, the probe DNA was hybridized with partially-complementary linker DNA strands which were loaded on AuNP surface *via* T–Hg^{2+}–T interaction. To achieve signal amplification, the AuNPs were modified with abundant guanine-rich oligonucleotide strands, which facilitated the intercalation of electroactive label methylene blue (MB). The enrichment of AuNPs and MB molecules on the electrode surface resulted in the intense signal increase, making the detection limit of Hg^{2+} down to 0.5 nM. Meanwhile, due to the specific T–Hg^{2+}–T interaction, the fabricated biosensor possessed high selectivity for the detection of mixed sample containing 10 times higher concentration of other environmentally-relevant divalent metal ions [97]. In addition, various groups have also utilized other ion-stabilized C-C mismatches (e.g. C-Ag^{+}-C mismatch) as well as some other specific DNA-ion interactions including DNAzyme [123], and G-quadruplexes which bind to Pb^{2+} and K^{+} respectively, to fabricate DNA-based metal ion biosensors for environmental and biomedical applications [124].

In recent years, aptamers, which are synthetic and highly-structured oligonucleotides binding to their targets, have been widely employed in molecular recognition [125, 126]. Similar as antibodies, aptamers possess high affinity against large number of targets including cytokines, proteases, immunoglobulins, small biological molecules, inorganic ions and even cells [127, 128]. But the advantages of aptamers (easy synthesis and chemical modification, low molecular weight and stability) make aptamers more accessible for the integration with NMNP surface. Another attractive feature about aptamers is that their recognition with targets often induces conformational changes (folding/unfolding) of biomolecules. Coupling of such variation with NMNPs would facilitate the generation of reagentless biosensors with exceptional sensitivity and selectivity [129, 130]. Typically, aptamers (or complementary ssDNA strands of aptamers) are conjugated with electroactive labels in the end and immobilized onto electrode surface. Through the interaction between aptamer and target molecules, they transform from flexible ssDNA to rigid conformation. As a result, the distance change between electroactive labels and electrode surface leads to the signal increase/decrease, which is correlated with the amount of targets. Mu's group utilized the architecture of DNA duplex, in which one strand worked as aptamer against and the other was labeled with ferrocene as signal-transducer. AuNPs were covered onto the SAM of p-aminothiophenol to enhance the surface area for anchoring more aptamers, and facilitate the electron transfer between ferrocene and electrode surface. In the presence of target lysozyme, the duplex de-hybridized due to the higher affinity between aptamer and lysozyme. Along with the release of complementary ssDNA into solution, the signal of ferrocene decreased, making the detection limit of lysozyme down to 1×10^{-13} M [96]. Fang's group utilized ferrocene-labeled aptamer to fabricate a switchable electrochemiluminescent (ECL) biosensor for the detection of thrombin, in which the aptamer worked as an identification element and ECL intensity switch. Without the target, aptamers formed spontaneous stem-loop structure, and the labeled ferrocene was able to quench the ECL intensity generated by the composite of AuNPs and ruthenium (II) tris-(bipyridine) ($Ru(bpy)_3^{2+}$) co-modified on the electrode surface. In the presence of target, however, the aptamer opened its stem-loop, so that the ferrocene was kept away from the ECL substrate and its quenching effect was weakened consequently [131].

Aptamers are able to work not only as recognition elements, their DNA structures are also advantageous to load large quantity of electroactive tags through electrostatic interaction or covalent labeling, which brings further signal amplification. Li's group fabricated a "sandwich" structure for the detection of platelet-derived growth factor-BB (PDGF), an important cytokine closely related to tumor growth with two independent aptamer-binding sites. The electrode surface was anchored with self-assembly monolayer of aptamers to capture target protein; meanwhile, AuNPs conjugated with aptamers were involved as recognition element and signal amplifiers. Each AuNP was loaded as many as 40 aptamers, and each strand was carrying up to 35 $[Ru(NH_3)_5Cl]^{2+}$ label molecules due to the electrostatic interaction between anionic phosphate groups and cationic labels. This structure induced strong signal amplification, and consequently the detection limit of 1×10^{-12} M could be obtained even for the detection of clinical serum samples [99]. Some groups combined different aptamers together and created novel "multi-functional" aptamer sequence for sequential or simultaneous detection of multiple targets [132, 133]. For instance, the adenosine aptamer-containing DNA sequence (S1) was designed to be complementary with lysozyme aptamer (S2) and another short ssDNA sequence (S3). S1 was immobilized onto the electrode surface and subsequently hybridized with S2 and S3, which was conjugated with AuNPs. Once either target (adenosine/lysozyme) was introduced into the system,

the higher affinity between aptamer and target resulted in the de-hybridization of DNA duplex and the release of AuNPs into the solution. The electrochemical signal decreased ~42% more than the control without AuNPs, and the detection limit of the biosensor was correspondingly ten times lower [134].

Immunosensors

Electrochemical immunoassay has demonstrated its broad applications for the fast, sensitive and selective detection of immunogens with simple instrumentation and low cost. Similar with the working mechanism of enzyme-linked immunosorbent assay (ELISA), most of electrochemical immunosensors are based on the sandwich-like immunocomplex composed of 1) capture antibody immobilized onto substrate surface; 2) target antigen in blood/serum/urine sample; and 3) detection antibody for signal output. Table 3 summarizes recent approaches for the construction of electrochemical immunosensors, in which NMNPs play significant roles both in the recognition of immunoreagents and the signal transduction/amplification processes. Due to the amplification effect of NMNPs as well as the utilization of electrochemical strategy, NMNP-based immunoassays are superior to ELISA, with exceeding detection sensitivity and specificity. For the detection of alpha-fetoprotein (α-AFP) as an example, the detection limit of NMNP-based electrochemical immunosensors is up to 10^7 magnitudes lower than commercially-available ELISA kit (LOD of α-AFP=2.0×10^{-9} g·mL^{-1}[135]).

Tumor markers (also called as tumor-related antigens) in blood, urine or tissue play important roles in cancer occurrence, growth and metastasis, so the level of tumor markers has been considered as the response to the presence of cancer or certain benign conditions. Immunoassays for the monitoring of tumor markers have been developed for early-stage cancer screening, diagnosis, evaluation of cancer development and therapy effects. As listed in Table 3, variety of tumor markers e.g. carcinoembryonic antigen (CEA), alpha-fetoprotein (α-AFP), prostate specific antigen (PSA) and interleukin-6 (IL-6) could be detected by electrochemical strategies. For instance, Ying and co-workers immobilized anti-PSA capture antibody on the electrode and conjugated detection antibody onto PtNP surface respectively, so that PtNPs could be anchored onto the electrode surface in the presence of target. To further amplify the electrochemical signal, the resulted electrode was then immersed into the PtNP growth solution containing $PtCl_4^{2-}$ and reductant. With the enlargement of PtNPs the signal generated by PtNP-catalyzed H_2O_2 reduction was also increased. Moreover, to design a progastrin releasing-peptide (ProGRP) immunosensor for the screening of small cell lung cancer, Yuan's group fabricated an electrochemical label by synthesizing nanocomposite of AuNPs and TiO_2 which possessed large surface area to load with antibodies conjugated with ferrocene and glucose oxidase (GOx) for signal amplification. In addition, the substrate electrode was modified with a nanostructured graphene sheet/AuNP/Nafion/cysteine composite membrane in order to get maximum immobilization of capture antibody and improve the electronic transmission rate. By measuring the redox signal of ferrocene with the catalysis of GOx, the obtained current is linear with the concentration of ProGRP in the concentration range from 1×10^{-11} to 5×10^{-10} g·mL^{-1}, and the obtained detection limit was down to 3×10^{-12} g·mL^{-1}[160].

In recent years, multiplexed tumor marker immunoassays which are able to detect two or more species of tumor markers simultaneously/sequentially have received more attention. Compared with single-analyte assays, they possess the advantages of shortened analysis time, improved detection efficiency, decreased sample volume and reduced costs. But these assays have high requirement for multiple signal output, which means each target needs an identified output signal without overlaying with others, and these signal outputs should be available in easily understandable form from single/multi channels. Correspondingly, there are two general strategies for multiplexed electrochemical immunoassays. The first one is based on spatially-separated reaction zones, such as independent electrodes and microarray systems [168]. Ju's group took advantage of screen-printed carbon electrode (SPCE) system containing two independent working electrodes and modified them with anti-CEA and anti-AFP antibodies respectively. For signal output, streptavidin-functionalized AgNP-enriched CNTs were designed as trace tags and were further enlarged by a subsequent Ag NP-promoted deposition of silver from enhancer solution to obtain simultaneous electrochemical-stripping signals of AgNPs on the two working electrodes [146]. In addition, the usage of multi-labels is an alternative way of signal output for multiplexed immunoassays. Song et al. synthesized thionine-labeled anti-AFP and ferrocene-labeled anti-CEA antibodies as redox probes. Each individual immunoreaction yielded a distinct differential pulse voltammetric (DPV) peak; the position and current value identified the species and concentration of the corresponding antigen. Pt hollow nanoparticles and HRP were also introduced for signal amplification. PtNPs conjugated with both HRP and electrochemical probe-labeled antibody acted as detecting element and catalyzed the reduction of H_2O_2 when they were anchored onto the electrode surface. As a result, the oxidation of thionine and ferrocene generated the signals respectively at the potentials of −0.15 V and 0.38 V, corresponding to the presence of AFP and CEA antigens [169]. Recently, to accomplish the continuous, in situ and rapid measurement of multiple analytes, microfluidic technology has been integrated with electrochemical immunosensors. Zhou et al. utilized the composite film of

Table 3 NMNP-based electrochemical immunosensors

Immunogen	NMNPs	Electrode Modification	Electrochemical Labels for Signal Output and Amplification	Detection Approach	Performance	References
Alpha-fetoprotein (α-AFP)	AuNPs	anti-AFP/glutaraldehyde/thionine	AuNPs loaded on CNTs acted as nanolabels and nanocatalysts. The electrochemical signal was generated by the redox cycling of substrates p-introphenol and $NaBH_4$ with the calalysis of AuNP-CNTs and electron mediation of thionine	CV and DPV	LOD=8×10^{-16} g·mL^{-1}, LDR=8×10^{-16}–2×10^{-7} g·mL^{-1}	[136]
AFP	AuNPs	AuNPs/CNTs/chitosan	alkaline phosphatase (ALP)-labeled anti-AFP acted as catalyst for the reduction of 1-naphthyl phosphate (1-NP)	EIS, CV and amperometry	LOD=6×10^{-10} g·mL^{-1}, LDR=1×10^{-9}–5.5×10^{-8} g·mL^{-1}	[137]
AFP	PtNPs	LBL assembly of MWCNTs/Nafion composite film co-immobilized with $Ru(bpy)_3^{2+}$/Pt aggregates/PtNPs	resistance increase after immunoreaction lead to the decrease of ECL intensity	ECL	LOD=3.3×10^{-12} g·mL^{-1}, LDR=1×10^{-11}–1×10^{-8} g·mL^{-1}	[138]
AFP	AuNPs/AgNPs	thionine/AuNPs/AgNPs/graphene hybrid nanosheet/anti-AFP	AuNP-enclosed TiO_2 NPs carrying HRP-labeled 2nd antibody acted as labels. The signal was generated by catalysis of HRP.	DPV, CV and EIS	LOD=5×10^{-13} g·mL^{-1}, LDR=1×10^{-12}–2×10^{-7} g·mL^{-1}	[139]
AFP	AuNPs/PtNPs	AuNPs/anti-AFP	Ferrocene monocarboxylic-HRP conjugated on PtNPs acted as labels for rolling circle amplification. The signal was generated by the catalysis of HRP and PtNPs with the addition of H_2O_2	DPV	LOD=1.7×10^{-12} g·mL^{-1}, LDR=5×10^{-12}–2×10^{-9} g·mL^{-1}	[140]
Brevetoxin B (BTX-2)	AuNPs	BTX-2 BSA conjugate/AuNPs/ amine-terminated poly(amidoamine) dendrimers	The signal was generated by the catalysis of H_2O_2-o-phenylenediamine by anti-BTX-2 labeled with HRP.	CV and DPV	LOD=1×10^{-11} g·mL^{-1}, LDR=3×10^{-11}–8×10^{-9} g·mL^{-1}	[141]
CA-125	AuNPs	deposited AuNPs/cystamine/anti-CA 125	$[Fe(CN)_6]^{3-/4-}$	CV and DPV	LOD=1×10^{-10} g·mL^{-1}	[142]
cardiac troponin I (cTnI) and C-reactive protein (CRP)	AuNPs	poly(dimethylsiloxane) (PDMS)/ AuNPs/anti-cTnI+anti-CRP	CdTe QDs conjugated with anti-cTnI+ZnSe QDs conjugated with anti-CRP	SWV	LOD of cTnI=4×10^{-12} g·mL^{-1}, LDR=1×10^{-11}–5×10^{-8} g·mL^{-1}; LOD of CRP=2.2×10^{-10} g·mL^{-1}, LDR=5×10^{-10}–2×10^{-7} g·mL^{-1}	[143]
carcinoembryonic antigen (CEA)	AuNPs	PB/AuNP/anti-CEA	AuNP-enwrapped graphene nanocomposites conjugated with HRP-labeled anti-CEA	CV	LOD=1×10^{-11} g·mL^{-1}, LDR=5×10^{-11}–3.5×10^{-7} g·mL^{-1}	[144]
CEA	AuNPs	LBL assembly of AuNP/nickel hexacyanoferrates nanoparticles/ AuNP/anti-CEA	Electroactive nickel hexacyanoferrates nanoparticles	EIS and CV	LOD=1×10^{-10} g·mL^{-1}, LDR=5×10^{-10}–1×10^{-8} g·mL^{-1}; 1×10^{-8}–1.6×10^{-7} g mL^{-1}	[145]
CEA and AFP	AgNPs	antibody/chitosan	streptavidin-functionalized AgNP-enriched CNTs	LSV	LOD of CEA=9.3×10^{-14} g mL^{-1}; LOD of AFP=6.1×10^{-14} g mL^{-1}; LDR=1×10^{-13}–5×10^{-9} g mL^{-1}	[146]
Hepatitis B	AuNPs	immunocomplex formed by AuNPs and magnetic nanoparticles conjugated with antibodies respectively in the presence of antigen	Reduction of copper onto the AuNP surface	ASV	LOD=8.7×10^{-11} g mL^{-1}, LDR=1×10^{-10}–1.5×10^{-6} g mL^{-1}	[147]
Hepatitis B	AuNPs	positively charged poly(allylamine)-branched ferrocene (PAA-Fc)/ AuNPs/anti-hepatitis B	ferrocene	CV and DPV	LOD=4×10^{-11} g mL^{-1}, LDR=1×10^{-10}–1.5×10^{-7} g mL^{-1}	[148]
Human immunoglobulin G (IgG)	PtNPs	AuNPs/anti-IgG	polydopamine (PDA)/PtNPs/antibody bionanocomposites acted as labels. The signal was generated by the reduction of H_2O_2 catalyzed by the PtNPs	QCM and LSV	LOD=1.8×10^{-11} g mL^{-1}, LDR=5×10^{-11}–1×10^{-8} g mL^{-1}	[149]

Table 3 (continued)

Immunogen	NMNPs	Electrode Modification	Electrochemical Labels for Signal Output and Amplification	Detection Approach	Performance	References
IgG	AgNPs	IgG	anti-IgG labeled AgNPs	DPV	LOD=4×10^{-10} g mL^{-1}, LDR=1×10^{-9}–1×10^{-6} g mL^{-1}	[150]
insulin like growth factor-1 (IGF-1)	AuNPs	1,6-hexanedithiol (HDT)/AuNPs/ anti-IGF 1	$[Fe(CN)_6]^{3-/4-}$	CV and EIS	LOD=1.5×10^{-13} g mL^{-1}, LDR=1×10^{-12}–1.8×10^{-10} g·mL^{-1}	[151]
Interleukin-6 (IL-6)	AuNPs	poly(diallyldimethyl ammonium chloride) (PDDA)/glutathione-protected AuNPs/anti-IL-6	H_2O_2 reaction catalyzed by 2nd antibody-labeled HRP	amperometry	LOD=1×10^{-11} g·mL^{-1}, LDR=2×10^{-11}–4×10^{-9} g·mL^{-1}	[152]
IL-6	AuNPs	polydopamine-stabilized AuNPs/PDDA functionalized graphene sheets/antigen modified on electrically-heated carbon paste electrode	CNTs conjugated with CdTe QD and antibodies *via* LBL assembly	ASV	LOD=3.3×10^{-14} g·mL^{-1}, LDR=1×10^{-13}–1×10^{-10} g·mL^{-1}	[153]
neomycin (Neo)	AuNPs	AuNPs/poly-[2,5-di-(2-thienyl)-1H-pyrrole-1-(p-benzoic acid)] (pDPB)/anti-Neo	AuNPs conjugated with 2nd antibody and hydrazine were decorated onto MWCNTs and acted as labels. The signal was generated by the reduction of H_2O_2 catalyzed by hydrazine	CV and amperometry	LOD=$6.76\pm0.17\times10^{-9}$ g·mL^{-1}, LDR=1×10^{-8}–2.5×10^{-7} g·mL^{-1}	[154]
platelet-derived growth factor BB (PDGF-BB)	AgNPs	anti-PDGF	graphene oxide (GO)-initiated AgNP enhancement	CV and SWV	LOD=5×10^{-12} g·mL^{-1}, LDR=1×10^{-11}–1×10^{-7} g·mL^{-1}	[155]
prostate specific antigen (PSA)	AuNPs	densely packed AuNP platform/ anti-PSA	magnetic beads modified with HRP-labeled 2nd antibody acted as labels. The signal was generated by the catalysis of 2,2′-azino-bis-(3-ethylbenz-thiazoline-6-sulfonic acid) (ABTS) and H_2O_2	CV and rotating disk amperometry	LOD=5×10^{-13} g·mL^{-1}, LDR=1×10^{-10}–1.5×10^{-7} g·mL^{-1}	[156]
PSA	PtNPs	16-mercapto-1-hexadecanoic acid (16-MHA)/11-mercapto-1-undecanol (11-MUOH)/anti-PSA	2nd antibody-labeled PtNPs in platinum developer solution to generate bare platinum catalysts in close proximity to the electrode surface. The signal was generated by Pt-catalyzed hydrogen evolution reaction	CV	LOD=1×10^{-15} g·mL^{-1}, LDR=1×10^{-15}–1×10^{-12} g·mL^{-1}	[157]
PSA	AgNPs	micro-gapped interdigitated electrode array	Enzymatic AgNP deposition reaction	LSV	LOD=9×10^{-13} g·mL^{-1}, LDR=1×10^{-12}–1×10^{-6} g·mL^{-1}	[158]
α-Synuclein (α-SYN)	AuNPs	photoelectrochemically deposited AuNPs/TiO_2 nanotube	AuNPs conjugated with antibodies and GO_X	EIS and photoelectrochemical measurements	LOD=3.4×10^{-11} g·mL^{-1}, LDR=5×10^{-11}–1×10^{-7} g·mL^{-1}	[159]
Progastrin releasing-peptide (ProGRP)	AuNPs	graphene nanosheets/nafion/AuNP/ anti-ProGRP	TiO_2-AuNP nanocomposite conjugated with GO_X and ferrocene-labeled 2nd antibody	CV	LOD=3×10^{-12} g·mL^{-1}, LDR=1×10^{-11}–5×10^{-10} g·mL^{-1}	[160]
Escherichia coli (*E. Coli*)	AuNPs	Polystyrene (PS)/*E.Coli*	Core-shell Cu@Au NPs labeled with anti-*E. coli* were dissolved by oxidation and released Cu^{2+} ions acted as labels.	ASV	LOD=30 CFU·mL^{-1}, LDR=5×10^{-10}–1×10^{-8} g·mL^{-1}; 1×10^{-8}–1.6×10^{-9} g·mL^{-1}	[161]
Bacillus globigii (BG)	AgNPs	AgNP/anti-BG	AgNPs	CV	LOD=602 spores/mL, LDR=1×10^{2}–3.5×10^{4} spores/mL	[162]
Jurkat cells during early apoptosis	AuNPs	AnnexinV/AuNPs/1,6-hexanedithiol	The resistance change after the immobilization of cells onto electrode surface *via* interaction between annexin V and phosphatidylserine exposed on cell surface	EIS	Impedance on the electrode surface was linearly correlated to the ratio of apoptotic cells.	[163]
Burkitt's lymphoma cells	AuNPs	magnetic beads loaded with aptamers	AuNPs conjugated with complementary DNA strands and CdS QDs	ASV and ECL	LOD=67 cells/mL; LDR =1×10^{2}–1×10^{5} cells/mL	[164]
cancer-associated glycosylation	AuNPs	lectin/thioglycolic acid/MWCNTs/ electrodeposited AuNPs	AuNPs loaded with lectin and thionine	DPV	LDR=7.0×10^{3}–1.1×10^{5} cells/mL for five cell lines	[165]
Hela cervix cancer cells	AuNPs		Cells were immobilized through the interaction between ConA and mannosyl groups on cell	CV	LOD=5×10^{2} cells/mL; LDR=8.0×10^{2}–2.0×10^{7} cells/mL	[166]

Table 3 (continued)

Immunogen	NMNPs	Electrode Modification	Electrochemical Labels for Signal Output and Amplification	Detection Approach	Performance	References
		PDDA-functionalized nitrogen-doped carbon nanotubes thionine/AuNPs/ concanavalin A (ConA)	surface. The electrochemical signal was generated by the HRP-labeled P-glycoprotein antibodies			
Drug-sensitive leukemia K562/B.W. cells and drug-resistant K562/ ADM cells	AuNPs	AuNPs/polylactide nanofibers (PLA)	Impedance of immobilized cells	EIS and DPV	LOD of K562/B.W. cells=8.0×10^{2} cells/mL; LDR =1.6×10^{3}–5.0×10^{6} cells/mL	[167]

Abbreviation: *ABTS* 2,2′-azino-bis-(3-ethylbenz-thiazoline-6-sulfonic acid), *AFP* alpha-fetoprotein, *ALP* alkaline phosphatase, *ASV* anodic stripping voltammetry, *α-SYN* α-synuclein, *BG bacillus globigii*, *BTX-2* brevetoxin B, *CEA* carcinoembryonic antigen, *ConA* concanavalin A, *CRP* C-reactive protein, *cTnI* cardiac troponin I, *CV* cyclic voltammetry, *DPV* differential pulse voltammetry, *ECL* electrochemiluminescence, *E. Coli* Escherichia coli, *EIS* electrochemical impedance spectroscopy, *GO* graphene oxide, *HDT* 1,6-hexanedithiol, *HRP* horseradish peroxidase, *IgG* human immunoglobulin G, *IGF-1* insulin like growth factor-1, *LBL* layer-by-layer, *LDR* linear detection range, *IL-6* interleukin-6, *LOD* limit of detection, *LSV* linear sweep voltammetry, *MWCNTs* multi-wall carbon nanotubes, *Neo* neomycin, *P4A-Fc* poly(allylamine)-branched ferrocene, *PB prussian blue*, *PD4* polydopamine, *PDDA* poly(diallyldimethyl ammonium chloride), *PDGF-BB* platelet-derived growth factor-BB, *PDMS* poly(dimethylsiloxane), *pDPB* poly-[2,5-di-(2-thienyl)-1H-pyrrole-1- (p-benzoic acid)], *PLA* polylactide nanofibers, *ProGRP*progastrin releasing-peptide, *PS* polystyrene, *PSA* prostate specific antigen, *QCM* quartz crystal microbalance, *QD* quantum dot, *SWV* square wave voltammetry, *1-NP* 1-naphthyl phosphate, *16-MHA* 16-mercapto-1-hexadecanoic acid, *11-MUOH* 11-mercapto-1-undecanol

AuNPs and poly(dimethylsiloxane) (PDMS) to modify a microfluidic chip with two cardiac biomarker antibodies. CdTe and ZnSe quantum dots were conjugated with detection antibodies respectively. With the dissolving of CdTe and ZnSe quantum dots, $Cd^{2+}$and Zn^{2+} were detected by square-wave anodic stripping voltammetry to enable the simultaneous monitoring of two biomarkers in clinical serum samples [143].

Compared with quantitative detection of biomolecules, the monitoring of living microorganisms on cellular level is more valuable but challenging. As the building block of life, the differentiation, growth, apoptosis of cells directly reflect the metabolism of an organism. Unlike biomolecules, cells possess much larger size as well as complicated composition, and they are sensitive with the exposure to any environmental or mechanical change. All of these factors make it difficult to immobilize onto substrate surface without any loss of activity. Nowadays, plenty of groups are working on fabricating cell-based electrochemical immunosensors for the monitoring of living mammalian cells. On the one hand, it is feasible to immobilize living cells onto NMNP-modified interface by taking advantage of the biocompatibility and easy surface modification of NMNPs. On the other, the specific cell-surface components including receptors, carbohydrates and lipids could be identified by using NMNPs which are functionalized with capture antibodies or cell-type specific aptamers. For instance, the early apoptosis of cells could be monitored through the interaction between Annexin V and phosphatidylserine, which is translocated from the inner side of the plasma membrane to cell surface. Once the living cells during early apoptosis were captured by the Annexin V on the AuNP-modified electrode surface, the impedance was significantly increased due to the large size of cells, which could be quantified using electrochemical impedance spectroscopy (EIS) [163]. Other groups have functionalized AuNPs and integrated them with other nanomaterials to immobilize living cells and monitor protein glycosylation on the cell surface, one of the most abundant and structurally diverse post-translational modifications in organisms [165, 166]. The immobilization and recognition of living cells could be achieved by utilizing concanavalin A (ConA), a class of carbohydrate-binding protein which specifically recognizes various sugars, glycoproteins and glycolipids. For instance, to quantify the mannose expression on K562 human erythroleukemic cell surface, Ding et al. firstly modified the electrode with arginine-glycine-aspartic acid-serine tetra peptide-functionalized single walled carbon nanohorns (RGDS-SWNHs) (Fig. 5) [170]. The K562 human erythroleukemic cells were then captured onto electrode surface through the specific interaction between RGD peptides and cell-surface integrin. The presence of SWNHs enlarged the electrode surface for loading of RGD peptides and spontaneous adsorption of cells; additionally, their electrochemical conductivity facilitated the electron transfer near electrode

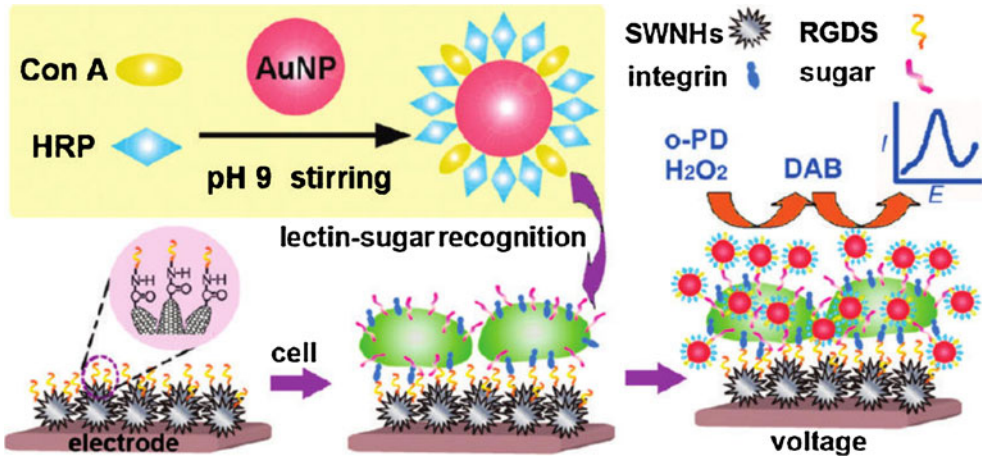

Fig. 5 Schematic description for in situ detection of mannose on K562 human erythroleukemic cells using AuNP nanoprobes and arginine-glycine-aspartic acid-serine tetra peptide-functionalized single walled carbon nanohorns (RGDS-SWNHs). Other abbreviations: Con A: concanavalin A; HRP: horseradish peroxidase; *o*-PD, *o*-phenylenediamine; DAB, 2,2′-diaminoazobenzene. (Reprinted with permission from ref. [170]. Copyright 2010 American Chemical Society)

surface. For signal output, AuNPs conjugated simultaneously with ConA and HRP molecules were working as detecting probes through the specific recognition between ConA and mannose on K562 cell surface, and the quantification of mannose was correlated with the DPV signals generated by the oxidation of substrate *o*-phenylenediamine (*o*-PD) catalyzed by HRP. The combination of AuNPs and SWNHs significantly enhanced the sensitivity of this immunosensor with a detection limit down to 15 cells in the volume of 10 μL. In addition, it allowed the monitoring of dynamic mannose expression change on living cell surface.

Electrochemical biosensors based on NMNP alloy

Heterostructured noble metal alloy contains two or more components, and their unique structures as well as intriguing chemical and physical properties make them applicable in various fields including electrochemistry, surface-enhanced Raman scattering (SERS), electrochemiluminescence and chemical catalysis. So far, a wide range of noble metal heterostructures (e.g. Au-Ag, Au-Pt, Pt-Pd, Pt-Ru) has been built up with designed shape and geometry [171, 172]. Ding's group developed Au-Ag bimetallic nanoporous tubes

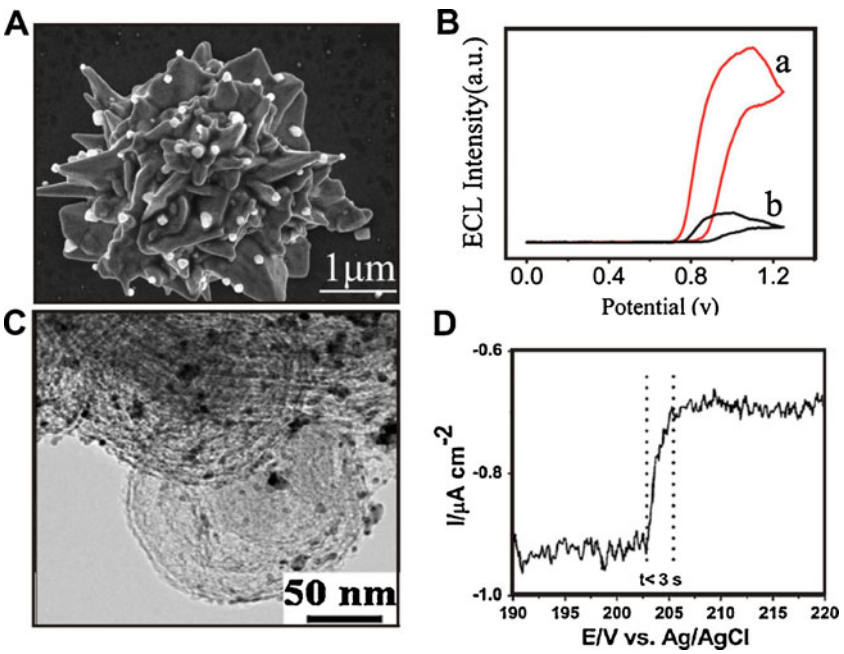

Fig. 6 **a**) Scanning electron microscopy (SEM) image of Au-Ag flower-dewdrop heterostructure. **b**) ECL potential scanning curves of Au-Ag flower-dewdrop structure-modified electrode (**a**) and a pure Au flower-decorated electrode (**b**) in 0.1 M PBS (pH 7.0) containing 1 mM $H_2C_2O_4$. Scan rate: 100 mVs^{-1}. **c**) SEM image of onion-like Pt-Pd- mesoporous carbon vesicle (MCV) alloy. **d**) The response time of Pt-Pd-MCV/Nafion-modified electrode towards the oxidation of glucose. (Fig. 6a&b are adapted with permission from ref. [174]. Copyright 2009 American Chemical Society; Fig. 6c&d are adapted with permission from ref. [181]. Copyright 2011 Elsevier)

via a three-step nanocrystal growth and structure-tailoring process [173]. The synthesized Ag nanowire worked as core followed by deposition of Au layer to form Au/Ag surface alloy. Through the etching process in nitric acid, Ag could be controllably leached out, leaving well-defined nanoporous structure. Their surface area provided large space for the immobilization of probe molecules. More interestingly, these Au-Ag nanotubes exhibited effective enhancement of ECL signal amplification due to the intense plasmon resonance of Au and Ag. When the nanotubes were tethered on the electrode surface, the modified electrode displayed remarkably one order of magnitude higher ECL signal at the oxidation potential of ECL label $Ru(bpy)_3^{2+}$ molecules compared with bare Au electrode. Besides of nanotubes, the Au-Ag alloy could be built up into flower-dewdrop heterostructure [174], in which the formed Ag nanodewdrop could be identified distinctly from the Au flowers (Fig. 6a), and it also enhanced the ECL intensity of $Ru(bpy)_3^{2+}$ when modified onto electrode surface (Fig. 6b), indicating their potential applications in the fabrication of sensitive electrochemical and ECL biosensors.

The Pt-Pd alloy has been employed as important catalysts for many electrochemical reactions including oxygen reduction [175, 176], methanol oxidation [177] and oxidation of glucose. Furthermore, the Pt-Pd alloy could be incorporated with carbon nanotubes [178] and polymers [179] to create novel chemical properties. Different groups have developed the nanocomposite of Pt-Pd alloy with highly-ordered mesoporous carbon vesicles for the electrochemical detection of hydrazine, hydrogen peroxide [180] and non-enzymatic catalysis of glucose [181]. Onion-like mesoporous carbon vesicle with multilayer lamellar structure possessed large surface area and pore volume (Fig. 6c), facilitating the modification of Pt-Pd alloy and the diffusion of glucose near the electrode surface. Additionally, the presence of bimetallic structure had strong electrocatalytic property and conductivity, which contributed to the rapid amperometric response towards the oxidation of glucose in 3 s (Fig. 6d).

Conclusion and perspective

Achieving strong sensitivity, efficiency, selectivity and simplicity has been always the driving forces for the biosensor design for a long time. As we have outlined in this review, the integration of noble metal nanomaterials has inspired the rapid development of electrochemical sensing approaches. On the one hand, NMNPs which are modified on electrode surface provide large surface area, rapid mass transport, facilitated electron transfer, effective catalysis and well control over local microenvironment. In addition, the highly-ordered assembly between NMNPs and biological molecules utilizing various surface modification methods, as well as the incorporation of NMNPs with other nanomaterials and polymers tremendously strengthen their advantages. On the other hand, the biocompatibility of NMNPs makes them suitable signal transducer and amplifier by carrying biological molecules, electroactive tags, redox complexes and metal ions. All these remarkable signal amplification strategies push the electrochemical biosensors capable of detecting hundreds of biological molecules or several living cells in liter volume of sample, and exhibit impressive selectivity even in the presence of excessive interferences or complex media.

Within the past decades, the concept of NMNPs has been expanded due to more effort in the morphological control of noble nanoparticles. Versatile nanostructures including nanocages [182], nanowires [183], nanorods [184], nanocubes [185], nanoflowers [186], nanotrees [187] and nanoprisms [188] possess exceeding optical, electronic and catalytic properties compared with traditional nanospheres [189, 190], and have been involved into the fabrication of electrochemical biosensors in recent years. For example, the roughness-controlled gold nanoflowers exhibit high electrocatalytic activity toward H_2O_2 and O_2, which could be attributed to the large active surface area [191]. Similarly, highly-branched silver nanodendrite could significantly increase the electron-transfer rate of electrochemical reactions when modified onto electrode surface [192]. As a fact, thousands of electrochemical biosensors based on different size, shape and surface modification of NMNPs have been presented or published in the nearest 3 years. However, it is still challenging to transduce them into commercially available apparatus. To accomplish this, the sophisticated surface functionalization of NMNPs is needed to improve the modification efficiency, solubility and long-term stability under different chemical, physiological and mechanical conditions. Furthermore, since the cost benefit is also an important concern of biosensor design, more effort would be put into the design of reusable sensors or cost-effective disposable sensors. In recent years, microfluidic devices and microarrays have integrated with electrochemical detection platforms and become a powerful tool to achieve the sample economy, high throughput, miniaturization and automation. By coupling the capabilities of NMNPs with the miniaturized detection system, it is predictable that novel generation of electrochemical sensing platforms would have great potential in a wide range of applications.

References

1. Willner I, Willner B (2010) Biomolecule-based nanomaterials and nanostructures. Nano Lett 10(10):3805–3815
2. Daniel MC, Astruc D (2004) Gold nanoparticles: assembly, supramolecular chemistry, quantum-size-related properties, and applications toward biology, catalysis, and nanotechnology. Chem Rev 104(1):293–346

3. El-Sayed MA (2001) Some interesting properties of metals confined in time and nanometer space of different shapes. Accounts Chem Res 34(4):257–264
4. Wang J, Yang LL, Boriskina S, Yan B, Reinhard BM (2011) Spectroscopic Ultra-trace detection of nitroaromatic gas vapor on rationally designed Two-dimensional nanoparticle cluster arrays. Anal Chem 83(6):2243–2249
5. Eustis S, El-Sayed MA (2006) Why gold nanoparticles are more precious than pretty gold: noble metal surface plasmon resonance and its enhancement of the radiative and nonradiative properties of nanocrystals of different shapes. Chem Soc Rev 35(3):209–217
6. Wang J, Boriskina SV, Wang HY, Reinhard BM (2011) Illuminating epidermal growth factor receptor densities on filopodia through plasmon coupling. Acs Nano 5(8):6619–6628
7. Guo SJ, Wang EK (2007) Synthesis and electrochemical applications of gold nanoparticles. Anal Chim Acta 598(2):181–192
8. Cao YWC, Jin RC, Mirkin CA (2002) Nanoparticles with Raman spectroscopic fingerprints for DNA and RNA detection. Science 297(5586):1536–1540
9. Nie SM, Emery SR (1997) Probing single molecules and single nanoparticles by surface-enhanced Raman scattering. Science 275(5303):1102–1106
10. Aslan K, Badugu R, Lakowicz JR, Geddes CD (2005) Metal-enhanced fluorescence from plastic substrates. J Fluoresc 15 (2):99–104
11. Zhang J, Lakowicz JR (2005) Enhanced luminescence of phenylphenanthridine dye on aggregated small silver nanoparticles. J Phys Chem B 109(18):8701–8706
12. Huang T, Murray RW (2003) Luminescence of tiopronin monolayer-protected silver clusters changes to that of gold clusters upon galvanic core metal exchange. J Phys Chem B 107 (30):7434–7440
13. Taleb A, Petit C, Pileni MP (1997) Synthesis of highly monodisperse silver nanoparticles from AOT reverse micelles: a way to 2D and 3D self-organization. Chem Mater 9(4):950–959
14. Wei H, Chen CG, Han BY, Wang EK (2008) Enzyme colorimetric assay using unmodified silver nanoparticles. Anal Chem 80 (18):7051–7055
15. Cao Y, Wang J, Xu YY, Li GX (2010) Sensing purine nucleoside phosphorylase activity by using silver nanoparticles. Biosens Bioelectron 25(5):1032–1036
16. Doty RC, Tshikhudo TR, Brust M, Fernig DG (2005) Extremely stable water-soluble Ag nanoparticles. Chem Mater 17(18):4630–4635
17. Lee JS, Lytton-Jean AKR, Hurst SJ, Mirkin CA (2007) Silver nanoparticle-oligonucleotide conjugates based on DNA with triple cyclic disulfide moieties. Nano Lett 7(7):2112–2115
18. Naik RR, Stringer SJ, Agarwal G, Jones SE, Stone MO (2002) Biomimetic synthesis and patterning of silver nanoparticles. Nat Mater 1(3):169–172
19. Peng ZM, Yang H (2009) Designer platinum nanoparticles: control of shape, composition in alloy, nanostructure and electrocatalytic property. Nano Today 4(2):143–164
20. Cao Y, Wang J, Xu YY, Li GX (2010) Combination of enzyme catalysis and electrocatalysis for biosensor fabrication: application to assay the activity of indoleamine 2,3-dioxygensae. Biosens Bioelectron 26(1):87–91
21. Polsky R, Gill R, Kaganovsky L, Willner I (2006) Nucleic acid-functionalized Pt nanoparticles: catalytic labels for the amplified electrochemical detection of biomolecules. Anal Chem 78 (7):2268–2271
22. Cao XD, Ye YK, Liu SQ (2011) Gold nanoparticle-based signal amplification for biosensing. Anal Biochem 417(1):1–16
23. Wang F, Hu SS (2009) Electrochemical sensors based on metal and semiconductor nanoparticles. Microchimica Acta 165(1–2):1–22
24. Pingarron JM, Yanez-Sedeno P, Gonzalez-Cortes A (2008) Gold nanoparticle-based electrochemical biosensors. Electrochim Acta 53(19):5848–5866
25. Privett BJ, Shin JH, Schoenfisch MH (2010) Electrochemical sensors. Anal Chem 82(12):4723–4741
26. Gooding JJ, Ciampi S (2011) The molecular level modification of surfaces: from self-assembled monolayers to complex molecular assemblies. Chem Soc Rev 40(5):2704–2718
27. Das J, Huh CH, Kwon K, Park S, Jon S, Kim K, Yang H (2009) Comparison of the nonspecific binding of DNA-Conjugated Gold nanoparticles between polymeric and monomeric Self-assembled monolayers. Langmuir 25(1):235–241
28. Liu GZ, Luais E, Gooding JJ (2011) The fabrication of Stable Gold Nanoparticle-modified interfaces for electrochemistry. Langmuir 27(7):4176–4183
29. Wang J, Zhou ND, Zhu ZQ, Huang JY, Li GX (2007) Detection of flavonoids and assay for their antioxidant activity based on enlargement of gold nanoparticles. Anal Bioanal Chem 388(5–6):1199–1205
30. Zhou N, Wang J, Chen T, Yu ZG, Li GX (2006) Enlargement of gold nanoparticles on the surface of a self-assembled monolayer modified electrode: A mode in biosensor design. Anal Chem 78 (14):5227–5230
31. Gao SY, Wu ZX, Pan DM, Lin Z, Cao R (2011) Preparation and characterization of polyoxometalate-Ag nanoparticles composite multilayer films. Thin Solid Films 519(7):2317–2322
32. Zhang S, Shao YY, Yin GP, Lin YH (2011) Self-assembly of Pt nanoparticles on highly graphitized carbon nanotubes as an excellent oxygen-reduction catalyst. Appl Catal, B-Environ 102(3–4):372–377
33. Zhang S, Shao YY, Yin GP, Lin YH (2010) Electrostatic Self-assembly of a Pt-around-Au nanocomposite with high activity towards formic acid oxidation. Angew Chem Int Ed 49(12):2211–2214
34. Pumera M, Ambrosi A, Bonanni A, Chng ELK, Poh HL (2010) Graphene for electrochemical sensing and biosensing. Trac-Trends Anal Chem 29(9):954–965
35. Zhu CZ, Guo SJ, Zhai YM, Dong SJ (2010) Layer-by-layer Self-assembly for constructing a Graphene/Platinum nanoparticle Three-dimensional Hybrid nanostructure using ionic liquid as a linker. Langmuir 26(10):7614–7618
36. Shan CS, Yang HF, Han DX, Zhang QX, Ivaska A, Niu L (2010) Graphene/AuNPs/chitosan nanocomposites film for glucose biosensing. Biosens Bioelectron 25(5):1070–1074
37. Feng XM, Li RM, Hu CH, Hou WH (2011) Direct electron transfer and electrocatalysis of hemoglobin immobilized on graphene-Pt nanocomposite. J Electroanal Chem 657(1–2):28–33
38. Guo SJ, Wen D, Zhai YM, Dong SJ, Wang EK (2010) Platinum nanoparticle Ensemble-on-Graphene hybrid nanosheet: One-pot, rapid synthesis, and used as new electrode material for electrochemical sensing. Acs Nano 4(7):3959–3968
39. Zhao W, Xu JJ, Chen HY (2006) Electrochemical biosensors based on layer-by-layer assemblies. Electroanalysis 18(18):1737–1748
40. Kim S, Park J, Cho J (2010) Layer-by-layer assembled multilayers using catalase-encapsulated gold nanoparticles. Nanotechnology 21 (37)
41. Zhu AW, Tian Y, Liu HQ, Luo YP (2009) Nanoporous gold film encapsulating cytochrome c for the fabrication of a H(2)O(2) biosensor. Biomaterials 30(18):3183–3188
42. Upadhyay S, Rao GR, Sharma MK, Bhattacharya BK, Rao VK, Vijayaraghavan R (2009) Immobilization of acetylcholineesterase-choline oxidase on a gold-platinum bimetallic nanoparticles modified glassy carbon electrode for the sensitive detection of organophosphate pesticides, carbamates and nerve agents. Biosens Bioelectron 25(4):832–838
43. Kim J, Lee SW, Hammond PT, Shao-Horn Y (2009) Electrostatic Layer-by-layer assembled Au Nano particle/MWNT thin films:

microstructure, optical property, and electrocatalytic activity for methanol oxidation. Chem Mater 21(13):2993–3001
44. Guo XH, Zheng D, Hu NF (2008) Enhancement of Au nanoparticles formed by in situ electrodeposition on direct electrochemistry of myoglobin loaded into Layer-by-layer films of chitosan and silica nanoparticles. J Phys Chem B 112(48):15513–15520
45. Facci T, Parreira RLT, Pereira-da-Silva MA, Oliveira ON, Huguenin F (2009) Pt/TiO(2)/poly(vinyl sulfonic acid) Layer-by-layer films for methanol electrocatalytic oxidation. J Nanosci Nanotechnol 9 (11):6620–6626
46. Palmero S, Colina A, Munoz E, Heras A, Ruiz V, Lopez-Palacios J (2009) Layer-by-layer electrosynthesis of Pt-Polyaniline nanocomposites for the catalytic oxidation of methanol. Electrochem Commun 11(1):122–125
47. Alencar WS, Crespilho FN, Martins MVA, Zucolotto V, Oliveira ON, Silva WC (2009) Synergistic interaction between gold nanoparticles and nickel phthalocyanine in layer-by-layer (LbL) films: evidence of constitutional dynamic chemistry (CDC). Phys Chem Chem Phys 11(25):5086–5091
48. Vercelli B, Zotti G, Berlin A (2009) Mono- and multilayers of platinum nanoparticles and Poly(3,4-ethylenedioxythiophene) as nanostructures for methanol electroxidation. J Phys Chem C 113 (9):3525–3529
49. Huang KJ, Sun JY, Jin CX, Jing QS, Zhou T (2011) Direct electrochemistry and electrocatalytic behavior of hemoglobin entrapped in chitosan/gold colloid/3-aminopropyl triethylene silane/Prussian blue composite film. Thin Solid Films 519 (11):3925–3930
50. Li MY, Huang SS, Zhu PS, Kong LM, Peng B, Gao H (2009) A novel DNA biosensor based on ssDNA/Cyt c/L-Cys/GNPs/Chits/GCE. Electrochim Acta 54(8):2284–2289
51. Lin JH, He CY, Zhao Y, Zhang SS (2009) One-step synthesis of silver nanoparticles/carbon nanotubes/chitosan film and its application in glucose biosensor. Sens Actuators B-Chem 137(2):768–773
52. Wen ZH, Ci SQ, Li JH (2009) Pt Nanoparticles inserting in carbon nanotube arrays: nanocomposites for glucose biosensors. J Phys Chem C 113(31):13482–13487
53. Gao LZ, Zhuang J, Nie L, Zhang JB, Zhang Y, Gu N, Wang TH, Feng J, Yang DL, Perrett S, Yan X (2007) Intrinsic peroxidase-like activity of ferromagnetic nanoparticles. Nat Nanotechnol 2 (9):577–583
54. Chang Q, Deng KJ, Zhu LH, Jiang GD, Yu C, Tang HQ (2009) Determination of hydrogen peroxide with the aid of peroxidase-like Fe(3)O(4) magnetic nanoparticles as the catalyst. Microchimica Acta 165(3–4):299–305
55. Yu FQ, Huang YZ, Cole AJ, Yang VC (2009) The artificial peroxidase activity of magnetic iron oxide nanoparticles and its application to glucose detection. Biomaterials 30(27):4716–4722
56. Zhuo Y, Yuan PX, Yuan R, Chai YQ, Hong CL (2009) Bienzyme functionalized three-layer composite magnetic nanoparticles for electrochemical immunosensors. Biomaterials 30(12):2284–2290
57. Qiu JD, Peng HP, Liang RP, Xia XH (2010) Facile preparation of magnetic core-shell Fe(3)O(4)@Au nanoparticle/myoglobin biofilm for direct electrochemistry. Biosens Bioelectron 25(6):1447–1453
58. Wang J, Cao Y, Xu YY, Li GX (2009) Colorimetric multiplexed immunoassay for sequential detection of tumor markers. Biosens Bioelectron 25(2):532–536
59. Li JP, Gao HL, Chen ZQ, Wei XP, Yang CF (2010) An electrochemical immunosensor for carcinoembryonic antigen enhanced by self-assembled nanogold coatings on magnetic particles. Anal Chim Acta 665(1):98–104
60. de la Escosura-Muniz A, Costa MMD, Merkoci A (2009) Controlling the electrochemical deposition of silver onto gold nanoparticles: Reducing interferences and increasing the sensitivity of magneto-immuno assays. Biosens Bioelectron 24(8):2475–2482
61. Caruso RA, Antonietti M (2001) Sol-gel nanocoating: an approach to the preparation of structured materials. Chem Mater 13(10):3272–3282
62. Toledano R, Mandler D (2010) Electrochemical code position of thin gold nanoparticles/Sol-Gel nanocomposite films. Chem Mater 22(13):3943–3951
63. Taheri A, Noroozifar M, Khorasani-Motlagh M (2009) Investigation of a new electrochemical cyanide sensor based on Ag nanoparticles embedded in a three-dimensional sol-gel. J Electroanal Chem 628(1–2):48–54
64. Manivannan S, Ramaraj R (2009) Core-shell Au/Ag nanoparticles embedded in silicate sol-gel network for sensor application towards hydrogen peroxide. J Chem Sci 121(5):735–743
65. Kannan P, John SA (2010) Highly sensitive determination of hydroxylamine using fused gold nanoparticles immobilized on sol-gel film modified gold electrode. Anal Chim Acta 663 (2):158–164
66. Sharma MK, Agarwal GS, Rao VK, Upadhyay S, Merwyn S, Gopalan N, Rai GP, Vijayaraghavan R, Prakash S (2010) Amperometric immunosensor based on gold nanoparticles/alumina sol-gel modified screen-printed electrodes for antibodies to Plasmodium falciparum histidine rich protein-2. Analyst 135(3):608–614
67. Zhang HJ, Chen GH (2009) Potent antibacterial activities of Ag/TiO(2) nanocomposite powders synthesized by a One-Pot Sol-Gel method. Environ Sci Technol 43(8):2905–2910
68. Zhang ZJ, Xie YB, Liu Z, Rong F, Wang Y, Fu DG (2011) Covalently immobilized biosensor based on gold nanoparticles modified TiO(2) nanotube arrays. J Electroanal Chem 650 (2):241–247
69. Zhou KF, Zhu YH, Yang XL, Luo J, Li CZ, Luan SR (2010) A novel hydrogen peroxide biosensor based on Au-graphene-HRP-chitosan biocomposites. Electrochim Acta 55(9):3055–3060
70. Xiang C, Zou Y, Sun LX, Xu F (2009) Direct electrochemistry and enhanced electrocatalysis of horseradish peroxidase based on flowerlike ZnO-gold nanoparticle-Nafion nanocomposite. Sens Actuators B-Chem 136(1):158–162
71. Abad JM, Gass M, Bleloch A, Schiffrin DJ (2009) Direct electron transfer to a metalloenzyme redox center coordinated to a Monolayer-protected cluster. J Am Chem Soc 131(29):10229–10236
72. Li FH, Song JX, Li F, Wang XD, Zhang QX, Han DX, Ivaska A, Niu L (2009) Direct electrochemistry of glucose oxidase and biosensing for glucose based on carbon nanotubes@SnO(2)-Au composite. Biosens Bioelectron 25(4):883–888
73. Han XA, Zhu YH, Yang XL, Li CZ (2010) Amperometric glucose biosensor based on platinum nanoparticle encapsulated with a clay. Microchimica Acta 171(3–4):233–239
74. Li JJ, Yuan R, Chai YQ (2011) Simple construction of an enzymatic glucose biosensor based on a nanocomposite film prepared in one step from iron oxide, gold nanoparticles, and chitosan. Microchimica Acta 173(3–4):369–374
75. Barbadillo M, Casero E, Petit-Dominguez MD, Vazquez L, Pariente F, Lorenzo E (2009) Gold nanoparticles-induced enhancement of the analytical response of an electrochemical biosensor based on an organic-inorganic hybrid composite material. Talanta 80(2):797–802
76. Yu CM, Guo JW, Gu HY (2009) Direct electrochemical behavior of hemoglobin at surface of Au@Fe(3)O(4) magnetic nanoparticles. Microchimica Acta 166(3–4):215–220
77. Liu Y, Han T, Chen C, Bao N, Yu CM, Gu HY (2011) A novel platform of hemoglobin on core-shell structurally Fe(3)O(4)@Au nanoparticles and its direct electrochemistry. Electrochim Acta 56 (9):3238–3247
78. Zhang LY, Yi M (2009) Electrochemical nitrite biosensor based on the immobilization of hemoglobin on an electrode modified by multiwall carbon nanotubes and positively charged gold nanoparticle. Bioprocess Biosyst Eng 32(4):485–492

79. Wang YY, Chen XJ, Zhu JJ (2009) Fabrication of a novel hydrogen peroxide biosensor based on the AuNPs-C@SiO(2) composite. Electrochem Commun 11(2):323–326
80. Jia SS, Fei JJ, Tian T, Zhou FQ (2009) Reagentless biosensor for hydrogen peroxide based on the Immobilization of hemoglobin in platinum nanoparticles enhanced Poly(chloromethyl thiirane) Cross-linked Chitosan Hybrid film. Electroanalysis 21(12):1424–1431
81. Wei NN, Xin X, Du JY, Li JL (2011) A novel hydrogen peroxide biosensor based on the immobilization of hemoglobin on three-dimensionally ordered macroporous (3DOM) gold-nanoparticle-doped titanium dioxide (GTD) film. Biosens Bioelectron 26(8):3602–3607
82. Lu CL, Shen QM, Zhao XM, Zhu JJ, Guo XF, Hou WH (2010) Ag nanoparticles self-supported on Ag(2)V(4)O(11) nano-belts: Novel nanocomposite for direct electron transfer of hemoglobin and detection of H(2)O(2). Sens Actuators B-Chem 150(1):200–205
83. Li F, Feng Y, Wang Z, Yang LM, Zhuo LH, Tang B (2010) Direct electrochemistry of horseradish peroxidase immobilized on the layered calcium carbonate-gold nanoparticles inorganic hybrid composite. Biosens Bioelectron 25(10):2244–2248
84. Zhang YY, Yuan R, Chai YQ, Xiang Y, Hong CL, Ran XQ (2010) An amperometric hydrogen peroxide biosensor based on the immobilization of HRP on multi-walled carbon nanotubes/electro-copolymerized nano-Pt-poly(neutral red) composite membrane. Biochem Eng J 51(3):102–109
85. Wang Y, Ma XL, Wen Y, Duan GP, Ren W, Zhang ZR, Yang HF (2009) Electrochemistry and electrocatalytic properties of mixed assemblies of horseradish peroxidase, poly(diallyl dimethylammonium chloride) and gold nanoparticles on a glassy carbon electrode. Microchimica Acta 166(3–4):283–288
86. Villalonga R, Diez P, Yanez-Sedeno P, Pingarron JM (2011) Wiring horseradish peroxidase on gold nanoparticles-based nanostructured polymeric network for the construction of mediatorless hydrogen peroxide biosensor. Electrochim Acta 56(12):4672–4677
87. Chen SH, Fu P, Yin B, Yuan R, Chai YQ, Xiang Y (2011) Immobilizing Pt nanoparticles and chitosan hybrid film on polyaniline naofibers membrane for an amperometric hydrogen peroxide biosensor. Bioprocess Biosyst Eng 34(6):711–719
88. Gu M, Wang JW, Tu YF, Di JW (2010) Fabrication of reagentless glucose biosensors: A comparison of mono-enzyme GOD and bienzyme GOD-HRP systems. Sens Actuators B-Chem 148 (2):486–491
89. Wang W, Zhang TJ, Zhang DW, Li HY, Ma YR, Qi LM, Zhou YL, Zhang XX (2011) Amperometric hydrogen peroxide biosensor based on the immobilization of heme proteins on gold nanoparticles-bacteria cellulose nanofibers nanocomposite. Talanta 84(1):71–77
90. Cao W, Wei CM, Hu JB, Li QL (2008) Direct electrochemistry and electrocatalysis of myoglobin immobilized on gold nanoparticles/carbon nanotubes nanohybrid film. Electroanalysis 20 (17):1925–1931
91. Xie WT, Kong LL, Kan MX, Han DM, Wang XJ, Zhang HM (2010) Introduction of gold nanoparticles into Myoglobin-Nafion film for direct electrochemistry application. J Nanosci Nanotechnol 10(10):6720–6724
92. Xiao Y, Patolsky F, Katz E, Hainfeld JF, Willner I (2003) "Plugging into enzymes": nanowiring of redox enzymes by a gold nanoparticle. Science 299(5614):1877–1881
93. Li H, Sun ZY, Zhong WY, Hao N, Xu DK, Chen HY (2010) Ultrasensitive electrochemical detection for DNA arrays based on silver nanoparticle aggregates. Anal Chem 82(13):5477–5483
94. Bai YH, Li JY, Xu JJ, Chen HY (2010) Ultrasensitive electrochemical detection of DNA hybridization using Au/Fe(3)O(4) magnetic composites combined with silver enhancement. Analyst 135(7):1672–1679
95. Lai GS, Yan F, Wu J, Leng CA, Ju HX (2011) Ultrasensitive multiplexed immunoassay with electrochemical stripping analysis of silver nanoparticles catalytically deposited by gold nanoparticles and enzymatic reaction. Anal Chem 83(7):2726–2732
96. Li LD, Chen ZB, Zhao HT, Guo L, Mu XJ (2010) An aptamer-based biosensor for the detection of lysozyme with gold nanoparticles amplification. Sens Actuators B-Chem 149(1):110–115
97. Kong RM, Zhang XB, Zhang LL, Jin XY, Huan SY, Shen GL, Yu RQ (2009) An ultrasensitive electrochemical "turn-on" label-free biosensor for Hg(2+) with AuNP-functionalized reporter DNA as a signal amplifier. Chem Commun 37:5633–5635
98. Mao L, Yuan R, Chai YQ, Zhuo Y, Jiang W (2011) Potential controlling highly-efficient catalysis of wheat-like silver particles for electrochemiluminescence immunosensor labeled by nano-Pt@Ru and multi-sites biotin/streptavidin affinity. Analyst 136 (7):1450–1455
99. Wang J, Meng WY, Zheng XF, Liu SL, Li GX (2009) Combination of aptamer with gold nanoparticles for electrochemical signal amplification: Application to sensitive detection of platelet-derived growth factor. Biosens Bioelectron 24(6):1598–1602
100. Ahangar LE, Mehrgardi MA (2011) Nanoparticle-functionalized nucleic acids: A strategy for amplified electrochemical detection of some single-base mismatches. Electrochim Acta 56(6):2725–2729
101. Liu SN, Wu P, Li W, Zhang H, Cai CX (2011) Ultrasensitive and selective electrochemical identification of hepatitis C virus genotype 1b based on specific endonuclease combined with gold nanoparticles signal amplification. Anal Chem 83(12):4752–4758
102. Ting BP, Zhang J, Gao ZQ, Ying JY (2009) A DNA biosensor based on the detection of doxorubicin-conjugated Ag nanoparticle labels using solid-state voltammetry. Biosens Bioelectron 25 (2):282–287
103. Huang KJ, Niu DJ, Xie WZ, Wang W (2010) A disposable electrochemical immunosensor for carcinoembryonic antigen based on nano-Au/multi-walled carbon nanotubes-chitosans nanocomposite film modified glassy carbon electrode. Anal Chim Acta 659(1–2):102–108
104. Deng CY, Chen JH, Nie Z, Wang MD, Chu XC, Chen XL, Xiao XL, Lei CY, Yao SZ (2009) Impedimetric aptasensor with femtomolar sensitivity based on the enlargement of Surface-charged gold nanoparticles. Anal Chem 81(2):739–745
105. Wang J, Shan Y, Zhao WW, Xu JJ, Chen HY (2011) Gold nanoparticle enhanced electrochemiluminescence of CdS thin films for ultrasensitive thrombin detection. Anal Chem 83(11):4004–4011
106. Lai GS, Yan F, Ju HX (2009) Dual signal amplification of glucose oxidase-functionalized nanocomposites as a trace label for ultrasensitive simultaneous multiplexed electrochemical detection of tumor markers. Anal Chem 81(23):9730–9736
107. Zhao J, Zhang YY, Li HT, Wen YQ, Fan XY, Lin FB, Tan LA, Yao SZ (2011) Ultrasensitive electrochemical aptasensor for thrombin based on the amplification of aptamer-AuNPs-HRP conjugates. Biosens Bioelectron 26(5):2297–2303
108. Li XM, Fu PY, Liu JM, Zhang SS (2010) Biosensor for multiplex detection of two DNA target sequences using enzyme-functionalized Au nanoparticles as signal amplification. Anal Chim Acta 673 (2):133–138
109. Wang J, Cao Y, Li Y, Liang ZQ, Li GX (2011) Electrochemical strategy for detection of phosphorylation based on enzyme-linked electrocatalysis. J Electroanal Chem 656(1–2):274–278
110. Qian P, Ai SY, Yin HS, Li JH (2010) Evaluation of DNA damage and antioxidant capacity of sericin by a DNA electrochemical biosensor based on dendrimer-encapsulated Au-Pd/chitosan composite. Microchimica Acta 168(3–4):347–354
111. Zhang YZ, Zhang KY, Ma HY (2009) Electrochemical DNA biosensor based on silver nanoparticles/poly(3-(3-pyridyl) acrylic acid)/carbon nanotubes modified electrode. Anal Biochem 387 (1):13–19

112. Chai Y, Tian DY, Wang W, Cui H (2010) A novel electrochemiluminescence strategy for ultrasensitive DNA assay using luminol functionalized gold nanoparticles multi-labeling and amplification of gold nanoparticles and biotin-streptavidin system. Chem Commun 46(40):7560–7562
113. Hao RZ, Song HB, Zuo GM, Yang RF, Wei HP, Wang DB, Cui ZQ, Zhang ZP, Cheng ZX, Zhang XE (2011) DNA probe functionalized QCM biosensor based on gold nanoparticle amplification for Bacillus anthracis detection. Biosens Bioelectron 26(8):3398–3404
114. Zhang J, Ting BP, Jana NR, Gao ZQ, Ying JY (2009) Ultrasensitive electrochemical DNA biosensors based on the detection of a highly characteristic solid-state process. Small 5(12):1414–1417
115. Wang Q, Yang LJ, Yang XH, Wang KM, He LL, Zhu JQ (2011) Electrochemical biosensors for detection of point mutation based on surface ligation reaction and oligonucleotides modified gold nanoparticles. Anal Chim Acta 688(2):163–167
116. Du M, Yang T, Jiao K (2010) Immobilization-free direct electrochemical detection for DNA specific sequences based on electrochemically converted gold nanoparticles/graphene composite film. J Mater Chem 20(41):9253–9260
117. Mehrgardi MA, Ahangar LE (2011) Silver nanoparticles as redox reporters for the amplified electrochemical detection of the single base mismatches. Biosens Bioelectron 26(11):4308–4313
118. Das J, Yang H (2009) Enhancement of electrocatalytic Activity of DNA-Conjugated gold nanoparticles and its application to DNA detection. J Phys Chem C 113(15):6093–6099
119. Yan Dua SG, Dong S, Wang E (2011) An integrated sensing system for detection of DNA using new parallel-motif DNA triplex system and graphene–mesoporous silica–gold nanoparticle hybrids. Biomaterials 32(33):8584–8592
120. Hvastkovs EG, Buttry DA (2010) Recent advances in electrochemical DNA hybridization sensors. Analyst 135(8):1817–1829
121. Lauer GM, Walker BD (2001) Medical progress: hepatitis C virus infection. N Engl J Med 345(1):41–52
122. Zhu ZQ, Su YY, Li J, Li D, Zhang J, Song SP, Zhao Y, Li GX, Fan CH (2009) Highly sensitive electrochemical sensor for mercury(II) ions by using a mercury-specific oligonucleotide probe and gold nanoparticle-based amplification. Anal Chem 81(18):7660–7666
123. Yang XR, Xu J, Tang XM, Liu HX, Tian DB (2010) A novel electrochemical DNAzyme sensor for the amplified detection of Pb(2+) ions. Chem Commun 46(18):3107–3109
124. Zhang XB, Kong RM, Lu Y (2011) Metal ion sensors based on DNAzymes and related DNA molecules. In: Cooks RG, Yeung ES (eds) annual review of analytical chemistry, Vol 4, vol 4. Annual review of analytical chemistry. pp 105–128
125. Ellington A, Szostak JW (1990) In vitro selection of RNA molecules that bind specific ligands. Nature 346:818–822
126. Tuerk CGL (1990) Systematic evolution of ligands by exponential enrichment: RNA ligands to bacteriophage T4 DNA polymerase. Science 249(4968):505–510
127. Pestourie C, Tavitian B, Duconge F (2005) Aptamers against extracellular targets for in vivo applications. Biochimie 87(9–10):921–930
128. Wang J, Li GX (2011) Aptamers against cell surface receptors: selection. Mod Appl Curr Med Chem 18(27):4107–4116
129. Li D, Song SP, Fan CH (2010) Target-responsive structural switching for nucleic acid-based sensors. Accounts Chem Res 43(5):631–641
130. Golub E, Pelossof G, Freeman R, Zhang H, Willner I (2009) Electrochemical, photoelectrochemical, and surface plasmon resonance detection of cocaine using supramolecular aptamer complexes and metallic or semiconductor nanoparticles. Anal Chem 81(22):9291–9298
131. Wang XY, Dong P, Yun W, Xu Y, He PG, Fang YZ (2009) A solid-state electrochemiluminescence biosensing switch for detection of thrombin based on ferrocene-labeled molecular beacon aptamer. Biosens Bioelectron 24(11):3288–3292
132. Li XM, Liu JM, Zhang SS (2010) Electrochemical analysis of two analytes based on a dual-functional aptamer DNA sequence. Chem Commun 46(4):595–597
133. Wang J, Cao Y, Chen GF, Li GX (2009) Regulation of thrombin activity with a bifunctional aptamer and hemin: development of a new anticoagulant and antidote pair. ChemBioChem 10 (13):2171–2176
134. Deng CY, Chen JH, Nie LH, Nie Z, Yao SZ (2009) Sensitive bifunctional aptamer-based electrochemical biosensor for small molecules and protein. Anal Chem 81(24):9972–9978
135. http://www.panomics.com/downloads/25_4_CAELISAPI_1_v1.pdf.
136. Tang JA, Tang DP, Su BL, Huang JX, Qiu B, Chen GN (2011) Enzyme-free electrochemical immunoassay with catalytic reduction of p-nitrophenol and recycling of p-aminophenol using gold nanoparticles-coated carbon nanotubes as nanocatalysts. Biosens Bioelectron 26(7):3219–3226
137. Lin JH, He CY, Zhang LJ, Zhang SS (2009) Sensitive amperometric immunosensor for alpha-fetoprotein based on carbon nanotube/gold nanoparticle doped chitosan film. Anal Biochem 384(1):130–135
138. Cao YL, Yuan R, Chai YQ, Mao L, Yang X, Yuan SR, Yuan YL, Liao YH (2011) A Solid-state electrochemiluminescence immunosensor based on MWCNTs-Nafion and Ru(bpy)(3)(2+)/Nano-Pt Nanocomposites for detection of alpha-Fetoprotein. Electroanalysis 23(6):1418–1426
139. Su BL, Tang DP, Li QF, Tang J, Chen GN (2011) Gold-silver-graphene hybrid nanosheets-based sensors for sensitive amperometric immunoassay of alpha-fetoprotein using nanogold-enclosed titania nanoparticles as labels. Anal Chim Acta 692(1–2):116–124
140. Su HL, Yuan R, Chai YQ, Mao L, Zhuo Y (2011) Ferrocenemonocarboxylic-HRP@Pt nanoparticles labeled RCA for multiple amplification of electro-immunosensing. Biosens Bioelectron 26(11):4601–4604
141. Tang DAP, Tang JA, Su B, Chen GN (2011) Gold nanoparticles-decorated amine-terminated poly(amidoamine) dendrimer for sensitive electrochemical immunoassay of brevetoxins in food samples. Biosens Bioelectron 26(5):2090–2096
142. Das J, Kelley SO (2011) Protein detection using arrayed microsensor chips: tuning sensor footprint to achieve ultrasensitive readout of CA-125 in serum and whole blood. Anal Chem 83 (4):1167–1172
143. Zhou F, Lu M, Wang W, Bian ZP, Zhang JR, Zhu JJ (2010) Electrochemical immunosensor for simultaneous detection of dual cardiac markers based on a Poly(Dimethylsiloxane)-Gold nanoparticles composite microfluidic chip: a proof of principle. Clin Chem 56(11):1701–1707
144. Zhong ZY, Wu W, Wang D, Shan JL, Qing Y, Zhang ZM (2010) Nanogold-enwrapped graphene nanocomposites as trace labels for sensitivity enhancement of electrochemical immunosensors in clinical immunoassays: Carcinoembryonic antigen as a model. Biosens Bioelectron 25(10):2379–2383
145. Yuan YR, Yuan R, Chai YQ, Zhuo Y, Miao XM (2009) Electrochemical amperometric immunoassay for carcinoembryonic antigen based on bi-layer nano-Au and nickel hexacyanoferrates nanoparticles modified glassy carbon electrode. J Electroanal Chem 626(1–2):6–13
146. Lai GS, Wu J, Ju HX, Yan F (2011) Streptavidin-functionalized silver-nanoparticle-enriched carbon nanotube tag for ultrasensitive multiplexed detection of tumor markers. Adv Funct Mater 21 (15):2938–2943

147. Shen GY, Zhang Y (2010) Highly sensitive electrochemical stripping detection of hepatitis B surface antigen based on copper-enhanced gold nanoparticle tags and magnetic nanoparticles. Anal Chim Acta 674(1):27–31
148. Qiu JD, Huang H, Liang RP (2011) Biocompatible and label-free amperometric immunosensor for hepatitis B surface antigen using a sensing film composed of poly(allylamine)-branched ferrocene and gold nanoparticles. Microchimica Acta 174(1–2):97–105
149. Fu YC, Li PH, Wang T, Bu LJ, Xie QJ, Xu XH, Lei LH, Zou C, Chen JH, Yao SZ (2010) Novel polymeric bionanocomposites with catalytic Pt nanoparticles label immobilized for high performance amperometric immunoassay. Biosens Bioelectron 25 (7):1699–1704
150. Hao N, Li H, Long YT, Zhang L, Zhao XR, Xu DK, Chen HY (2011) An electrochemical immunosensing method based on silver nanoparticles. J Electroanal Chem 656(1–2):50–54
151. Rezaei B, Majidi N, Rahmani H, Khayamian T (2011) Electrochemical impedimetric immunosensor for insulin like growth factor-1 using specific monoclonal antibody-nanogold modified electrode. Biosens Bioelectron 26(5):2130–2134
152. Munge BS, Krause CE, Malhotra R, Patel V, Gutkind JS, Rusling JF (2009) Electrochemical immunosensors for interleukin-6. comparison of carbon nanotube forest and gold nanoparticle platforms. Electrochem Commun 11(5):1009–1012
153. Zhang JJ, Liu Y, Hu LH, Jiang LP, Zhu JJ (2011) "Proof-of-principle"' concept for ultrasensitive detection of cytokines based on the electrically heated carbon paste electrode. Chem Commun 47(23):6551–6553
154. Zhu Y, Son JI, Shim YB (2010) Amplification strategy based on gold nanoparticle-decorated carbon nanotubes for neomycin immunosensors. Biosens Bioelectron 26(3):1002–1008
155. Qu FL, Lu HM, Yang MH, Deng CY (2011) Electrochemical immunosensor based on electron transfer mediated by graphene oxide initiated silver enhancement. Biosens Bioelectron 26 (12):4810–4814
156. Mani V, Chikkaveeraiah BV, Patel V, Gutkind JS, Rusling JF (2009) Ultrasensitive immunosensor for cancer biomarker proteins using gold nanoparticle film electrodes and multienzyme-particle amplification. Acs Nano 3(3):585–594
157. Zhang J, Ting BP, Khan M, Pearce MC, Yang YY, Gao ZQ, Ying JY (2010) Pt nanoparticle label-mediated deposition of Pt catalyst for ultrasensitive electrochemical immunosensors. Biosens Bioelectron 26(2):418–423
158. Huang Y, Wang TH, Jiang JH, Shen GL, Yu RQ (2009) Prostate specific antigen detection using microgapped electrode array immunosensor with enzymatic silver deposition. Clin Chem 55 (5):964–971
159. An YR, Tang LL, Jiang XL, Chen H, Yang MC, Jin LT, Zhang SP, Wang CG, Zhang W (2010) A photoelectrochemical immunosensor based on Au-Doped TiO(2) nanotube arrays for the detection of alpha-synuclein. Chem-A Eur J 16(48):14439–14446
160. Zhuo Y, Chai YQ, Yuan R, Mao L, Yuan YL, Han J (2011) Glucose oxidase and ferrocene labels immobilized at Au/TiO(2) nanocomposites with high load amount and activity for sensitive immunoelectrochemical measurement of ProGRP biomarker. Biosens Bioelectron 26(9):3838–3844
161. Zhang XN, Geng P, Liu HJ, Teng YQ, Liu YJ, Wang QJ, Zhang W, Jin LT, Jiang L (2009) Development of an electrochemical immunoassay for rapid detection of E. coli using anodic stripping voltammetry based on Cu@Au nanoparticles as antibody labels. Biosens Bioelectron 24(7):2155–2159
162. Mwilu SK, Aluoch AO, Miller S, Wong P, Sadik OA (2009) Identification and quantitation of Bacillus globigii using metal enhanced electrochemical detection and capillary biosensor. Anal Chem 81(18):7561–7570
163. Tong CY, Shi BX, Xiao XJ, Liao HD, Zheng YQ, Shen GL, Tang DY, Liu XM (2009) An Annexin V-based biosensor for quantitatively detecting early apoptotic cells. Biosens Bioelectron 24(6):1777–1782
164. Ding CF, Ge Y, Zhang SS (2010) Electrochemical and electrochemiluminescence determination of cancer cells based on aptamers and magnetic beads. Chem-A Eur J 16(35):10707–10714
165. Zhang XA, Teng YQ, Fu Y, Xu LL, Zhang SP, He B, Wang CG, Zhang W (2010) Lectin-based biosensor strategy for electrochemical assay of glycan expression on living cancer cells. Anal Chem 82(22):9455–9460
166. Zhang JJ, Cheng FF, Zheng TT, Zhu JJ (2010) Design and implementation of electrochemical cytosensor for evaluation of cell surface carbohydrate and glycoprotein. Anal Chem 82 (9):3547–3555
167. Wu XJ, Jiang H, Zheng JS, Wang XM, Gu ZZ, Chen C (2011) Highly sensitive recognition of cancer cells by electrochemical biosensor based on the interface of gold nanoparticles/polylactide nanocomposites. J Electroanal Chem 656(1–2):174–178
168. Du D, Wang J, Lu DL, Dohnalkova A, Lin YH (2011) Multiplexed electrochemical immunoassay of phosphorylated proteins based on enzyme-functionalized gold nanorod labels and electric field-driven acceleration. Anal Chem 83(17):6580–6585
169. Song ZJ, Yuan R, Chai YQ, Zhuo Y, Jiang W, Su HL, Che X, Li JJ (2010) Horseradish peroxidase-functionalized Pt hollow nanospheres and multiple redox probes as trace labels for a sensitive simultaneous multianalyte electrochemical immunoassay. Chem Commun 46(36):6750–6752
170. Ding L, Ji QJ, Qian RC, Cheng W, Ju HX (2010) Lectin-based nanoprobes functionalized with enzyme for highly sensitive electrochemical monitoring of dynamic carbohydrate expression on living cells. Anal Chem 82(4):1292–1298
171. Sanchez SI, Small MW, Zuo JM, Nuzzo RG (2009) Structural characterization of Pt-Pd and Pd-Pt Core-Shell nanoclusters at atomic resolution. J Am Chem Soc 131(24):8683–8689
172. Xu J, White T, Li P, He CH, Yu JG, Yuan WK, Han YF (2010) Biphasic Pd-Au alloy catalyst for low-temperature CO oxidation. J Am Chem Soc 132(30):10398–10406
173. Gu XH, Xu LQ, Tian F, Ding Y (2009) Au-Ag Alloy nanoporous nanotubes. Nano Research 2(5):386–393
174. Gao L, Fan LZ, Zhang J (2009) Selective growth of Ag nanodewdrops on Au nanostructures: a new type of bimetallic heterostructure. Langmuir 25(19):11844–11848
175. Lim B, Jiang MJ, Camargo PHC, Cho EC, Tao J, Lu XM, Zhu YM, Xia YN (2009) Pd-Pt Bimetallic Nanodendrites with high activity for oxygen reduction. Science 324(5932):1302–1305
176. Peng ZM, Yang H (2009) Synthesis and oxygen Reduction Electrocatalytic Property of Pt-on-Pd bimetallic heteronanostructures. J Am Chem Soc 131(22):7542−+
177. Guo SJ, Dong SJ, Wang EW (2010) Three-Dimensional Pt-on-Pd bimetallic nanodendrites supported on graphene nanosheet: facile synthesis and used as an advanced nanoelectrocatalyst for methanol oxidation. Acs Nano 4(1):547–555
178. Xiao F, Zhao FQ, Mei DP, Mo ZR, Zeng BZ (2009) Nonenzymatic glucose sensor based on ultrasonic-electrode position of bimetallic PtM (M=Ru, Pd and Au) nanoparticles on carbon nanotubes-ionic liquid composite film. Biosens Bioelectron 24(12):3481–3486
179. Zhou ZL, Kang TF, Zhang Y, Cheng SY (2009) Electrochemical sensor for formaldehyde based on Pt-Pd nanoparticles and a Nafion-modified glassy carbon electrode. Microchimica Acta 164(1–2):133–138
180. Bo XJ, Bai J, Ju JA, Guo LP (2010) A sensitive amperometric sensor for hydrazine and hydrogen peroxide based on palladium nanoparticles/onion-like mesoporous carbon vesicle. Anal Chim Acta 675(1):29–35
181. Bo XJ, Bai J, Yang L, Guo LP (2011) The nanocomposite of PtPd nanoparticles/onion-like mesoporous carbon vesicle for

nonenzymatic amperometric sensing of glucose. Sens Actuators B-Chem 157(2):662–668
182. Xia YN, Li WY, Cobley CM, Chen JY, Xia XH, Zhang Q, Yang MX, Cho EC, Brown PK (2011) Gold Nanocages: from synthesis to theranostic applications. Accounts Chem Res 44(10):914–924
183. Holmes JD, Johnston KP, Doty RC, Korgel BA (2000) Control of thickness and orientation of solution-grown silicon nanowires. Science 287(5457):1471–1473
184. Yu YY, Chang SS, Lee CL, Wang CRC (1997) Gold nanorods: electrochemical synthesis and optical properties. J Phys Chem B 101(34):6661–6664
185. McLellan JM, Siekkinen A, Chen JY, Xia YN (2006) Comparison of the surface-enhanced Raman scattering on sharp and truncated silver nanocubes. Chem Phys Lett 427(1–3):122–126
186. Xie JP, Zhang QB, Lee JY, Wang DIC (2008) The synthesis of SERS-active gold nanoflower tags for In vivo applications. ACS NANO 2(12):2473–2480
187. Nadagouda MN, Polshettiwar V, Varma RS (2009) Self-assembly of palladium nanoparticles: synthesis of nanobelts, nanoplates and nanotrees using vitamin B(1), and their application in carbon-carbon coupling reactions. J Mater Chem 19(14):2026–2031
188. Jin RC, Cao YW, Mirkin CA, Kelly KL, Schatz GC, Zheng JG (2001) Photoinduced conversion of silver nanospheres to nanoprisms. Science 294(5548):1901–1903
189. Chen JY, Wiley B, McLellan J, Xiong YJ, Li ZY, Xia YN (2005) Optical properties of Pd-Ag and Pt-Ag nanoboxes synthesized via galvanic replacement reactions. Nano Lett 5(10):2058–2062
190. El-Sayed MA (2001) Some interesting properties of metals confined in time and nanometer space of different shapes. Accounts Chem Res 34(4):257–264
191. Shan CS, Han DX, Song JF, Ivaska A, Niu L (2010) Flowerlike submicrometer gold particles: Size- and surface roughness-controlled synthesis and electrochemical characterization. J Mater Res 25(9):1755–1760
192. Rezaei B, Damiri S (2010) Electrodeposited silver nanodendrites electrode with strongly enhanced electrocatalytic activity. Talanta 83(1):197–204